AN INVESTIGATION OF THE EFFECT OF VARIABLE PARAMETERS ON THE MATERIAL QUALITY IN TEMPCORE PROCESS

A Thesis Submitted to the
Graduate School of Natural and Applied Sciences of
Dokuz Eylül University
in Partial Fulfillment of the Requirements for
the Degree of Master of Science in Mechanical Engineering, Material Science Program
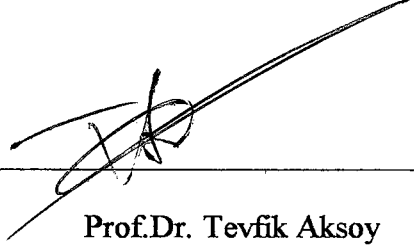
by
Hakan ÇETİNEL

January, 1997
İZMİR

M.Sc. THESIS EXAMINATION RESULT FORM

We certify that we have read this thesis and that in our opinion it is fully adequate, in scope and in quality, as a thesis for the degree of Master of Science.

Prof.Dr. Tevfik Aksoy
(Advisor)

Prof.Dr. Kazım ÖNEL
(Committee Member)

Prof.Dr. Ahmet ÇAKIR
(Committee Member)

Approved by the
Graduate School of Natural and Applied Sciences

Prof.Dr.Macit Toksoy
Director

ACKNOWLEDGMENTS

ABSTRACT

The Tempcore process used in recent years is applied for increasing the strength values of the concrete-reinforcing steel bars by quenching. This heat treatment process comprises three stages: a fast cooling step which is applied to the bar as near as possible to exit of the last finishing stand and leads to a quenched skin; a step during which the core reheats the quenched surface layer by conduction; an air cooling step, leading to quasi isothermal transformation of the remaining austenite of the core.

In this study; applicability of Tempcore method to materials having chemical composition of %0.16-0.21 C, %0.17-0.22 Si, %0.74-0.83 Mn has been examined by finite elements method and compared.with the results of the experiments. Heat transfer equations and amount of phase tranformation have been calculated by Fortran77 computer programme.

After tests and computer applications approving that test result; it has been seen that yield and tensile strengths of steel bars, having chemical compositions mentioned above, had increased and strain values had decreased. The cause of changes at these mechanical values is the martensitic layer on surface occured by quenching. By inner structure changes; heat capacity and conduction coefficient change, and these effects change the heat transfer characteristics of the material. In bars of different diameters exposed to Tempcore method, it has been seen that yield and tensile strengths had increased and the self-tempering temperature had increased in proportion to increasing duration of quenching. In practice, the change in internal structure can not be determined sensitively. In finite elements method, phase ratios for the each node can be calculated so it gives better results.

ÖZET

Son yıllarda kullanılmaya başlanan proseslerden olan Tempcore prosesi; nervürlü inşaat çeliklerine su verme işlemiyle dayanım değerlerinde artış sağlamak amacı ile kullanılmaktadır. Bu ısıl işlemi; haddeleme işleminin hemen ardından malzemeye su verilmesi daha sonra havada soğuma ve soğuma yatağında bekleme esnasında kendi kendini temperleme sürecini kapsamaktadır.

Bu araştırmada; %0.16-%0.21 C, %0.17-0.22 Si, %0.74-0.83 Mn kimyasal kompozisyon aralığındaki çelik çubuklarda Tempcore yönteminin uygulanabilirliği sonlu elemanlar yöntemiyle incelenmiştir. Isı transferi ve faz dönüşüm miktarları bilgisayarda Fortran77 programlama dili ile hesaplanmıştır.

Deneysel sonuçlar ve bu sonuçları belli toleranslar dahilinde destekleyen bilgisayarlı uygulama sonuçlarında; yukarıdaki kimyasal kompozisyon aralığındaki çelik çubuklarda akma ve çekme dayançlarının arttığı ancak uzama değerlerinin düştüğü görülmüştür. Bu mekanik değerlerin değişim nedeni; yüzeyde su verme nedeniyle oluşan ve su verme süresi arttıkça hacim yüzdesi artan martenzit kabuktur. İç yapı değişimi ile; ısıl kapasite ve kondüksiyon katsayısı değişmekte, bu etkenler ile de ısı transferi karakteristiği değişmektedir. Tempcore yöntemi uygulanan değişik çaplardaki çubuklarda; su verme süresindeki artış ile akma ve çekme mukavemetlerinin doğrusal yükseldiği, kendi kendini temperleme sıcaklığının doğrusal düştüğü görülmüştür. Pratikte, iç yapı değişimini hassas olarak tesbit etmek mümkün olmadığı ve sonlu elemanlar metodunda bütün düğümlerdeki faz oranı her iterasyonda hesaplandığı için metallografik muayeneden daha iyi sonuçlar vermektedir.

CONTENTS

Chapter One

INTRODUCTION

Chapter Two

THEORY OF THE TEMPCORE PROCESS

Chapter Three
HEAT TRANSFER AND FINITE ELEMENT MODELING

Chapter Four
TRANSITION FROM ISOTHERMIC T.T.T TO CONTINUOUS COOLING TRANSFORMATION (CCT) CURVES

Chapter Five
EXPERIMENTS, CALCULATIONS AND RESULTS

Chapter Six
CONCLUSIONS

LIST OF TABLES

LIST OF FIGURES

CHAPTER ONE
INTRODUCTION

The high yield strength concrete-reinforcing bars with improved adherence that are produced in west Europe can be subdivided into two distinct categories, viz.:

- "naturally hard" bars which are used in the as-rolled condition after cooling in still air;

- work-hardened bars which acquire their service properties by cold deformation through twisting, drawing or rolling.

From the user's view point these two categories of concrete-reinforcing bars differ in terms of weldability: for a given yield strength level, cold-worked bars, because of their lower carbon, manganese and silicon contents are easy to weld, i.e. their welding calls for less precautions than naturally hard bars.

Although it is possible to produce naturally hard bars with a low carbon content, and hence with a good weldability, this only be achieved through an addition of large quantities of niobium and vanadium, which boosts their cost price.(Economopoulos, & Respen, & Lessel, & Steffes, 1975).

The process, which involves applying a heat treatment from the heat of rolling, makes it possible to economically produce high yield strength concrete-reinforcing bars.

The designation "Tempcore" was adopted for the new process, since it reflects the principle on which it is based, viz. : tempering of a previously quenched surface layer, under the effect of heat supplied by the core of the product.

The applicability of Tempcore process to low carbon (%0,17-0.22 C) bearing reinforcing steel bars and its effect on mechanical properties has been studied. The process has been using for several years in İDÇ Sanayi A.Ş. rolling mill for notched bars. (Özsoyeller, 1993)

Some experimental work has been carried out using this process which comprises of two steps; These are surface quenching of the hot bar coming out of the last rolling stand and self-tempering of the quenched section. Experimental results have proved that the mechanical properties of low carbon bearing reinforcing bars can be improved and controlled via this process. It has been found out that for differing bar sizes increasing quenching time results in a linear increase in both yield and tensile strength and a linear decrease in tempering temperature.

The finite elements method gives the opportunity to change bar diameter, quenching time and initial temperature widely. Bars which have 16, 18, 20, 22 mm diameter have been quenched in different quenching time and the amount of martensite has determined for each nodes. As a result, appropriateness of strength values has been determined.

In the contents of this study; firstly, fundamental principles of Tempcore process has been introduced, then finite elements modeling has been done and finally its results have been compared with the test results.

Finite elements modeling of heat transfer equations, and amount of change in internal structures are solved by FORTRAN 77 programme.

CHAPTER TWO
THEORY OF THE TEMPCORE PROCESS

The purpose of this section is to analyse the fundamental physical phenomena underlying the Tempcore process and to discuss the effect of the more important independent variables on the final result of the Tempcore heat treatment, namely the mechanical properties of the treated bars.

2.1 Principle of the Process

Tempcore is a direct quenching and self-tempering process from the heat of rolling. The present description is exclusively devoted to the heat treatment of hot rolled concrete reinforcing bars.

According to the Tempcore process the concrete bar from the rolling mill is submitted to a special heat treating cycle involving three stages:

2.1.1 First Stage

The firs stage is a fast cooling operation applied to the bar as it leaves the last finishing stand. The efficiency of the cooling facility used in this first stage must be such that the cooling rate down to a certain depth below the skin is higher than the critical rate for martensitic quenching.

At the conclusion of this operation, the bar has an austenite core surrounded by a layer composed of a mixture of austenite and martensite, with the martensite content decreasing from the skin towards the inner. The aimed duration of the first stage depends on the desired thickness of the martensitic layer.

2.1.2 Second Stage

During the second stage, the bar leaves the area of drastic cooling and is exposed to air. The heat transfer coefficient of the environment being very small, and the temperature gradient within the bar's cross-section being very large, the core reheats the quenched surface layer by conduction. As a result, the martensite formed during the first stage is subjected to self-tempering which, as will be shown below, ensures adequate ductility while maintaining a high yield strength level.

The second stage is conventionally considered as terminated when the temperature at the surface of the bar passes through a maximum, called "Tempering Temperature". The duration of the second stage varies greatly with the bar diameter and the cooling conditions applied during the first stage.

In the course of the second stage, the untransformed austenite in the surface layer transforms to bainite, whereas the core remains austenitic. On the other hand, the austenite subjacent to the tempered martensite layer can start to transform to bainite, depending on the steel's composition and the cooling conditions.

2.1.3 Third Stage

The third stage occurs as the bar lies on the cooling bed. It consists of a quasi-isothermal transformation of the remaining austenite. The product of this transformation is a mixture of either ferrite and pearlite or ferrite, pearlite and bainite, depending on several factors, viz.:

- the steel composition;

- the bar diameter;

- the finishing temperature of the rolling sequence;

- the efficiency and duration of cooling during the first stage.

The physical phenomena involved in the above mentioned three stages of the Tempcore process can be divided in three categories:

a) heat exchanges between the surface of the bar and the surroundings;

b) heat conduction in the bar;

c) metallurgical phenomena such as allotropic transformations.

In the following sections, the effect of the governing parameters and the interrelations of the above phenomena will be discussed.

2.2 Fundamental Mechanisms of Tempcore Hardening

Figure 2.1 is a schematic representation of the fundamental mechanisms of Tempcore hardening and their interrelations (CRM, 1985). The involved phenomena have been divided as stated previously in three classes: surface heat exchanges, heat conduction and physical metallurgy (vertical dotted lines in the figure). On the top of the figure are represented, inside circles, the governing parameters of the process. Among them, only three can be considered as independent control variables from the point of view of the rolling mill operator, namely: the water flow rate, the quenching time and the finishing temperature.

In Tempcore treated bars, the microstructure and properties vary continuously from the surface to the axis of the bar. Nevertheless, it is possible, as a satisfactory approximation to consider the Tempcore bars as composed of two distinct parts : a surface layer that for the sake of simplicity, we shall name "Tempered Martensite" or "Mertensite" and the central part or "Core" composed of ferrite and carbides.
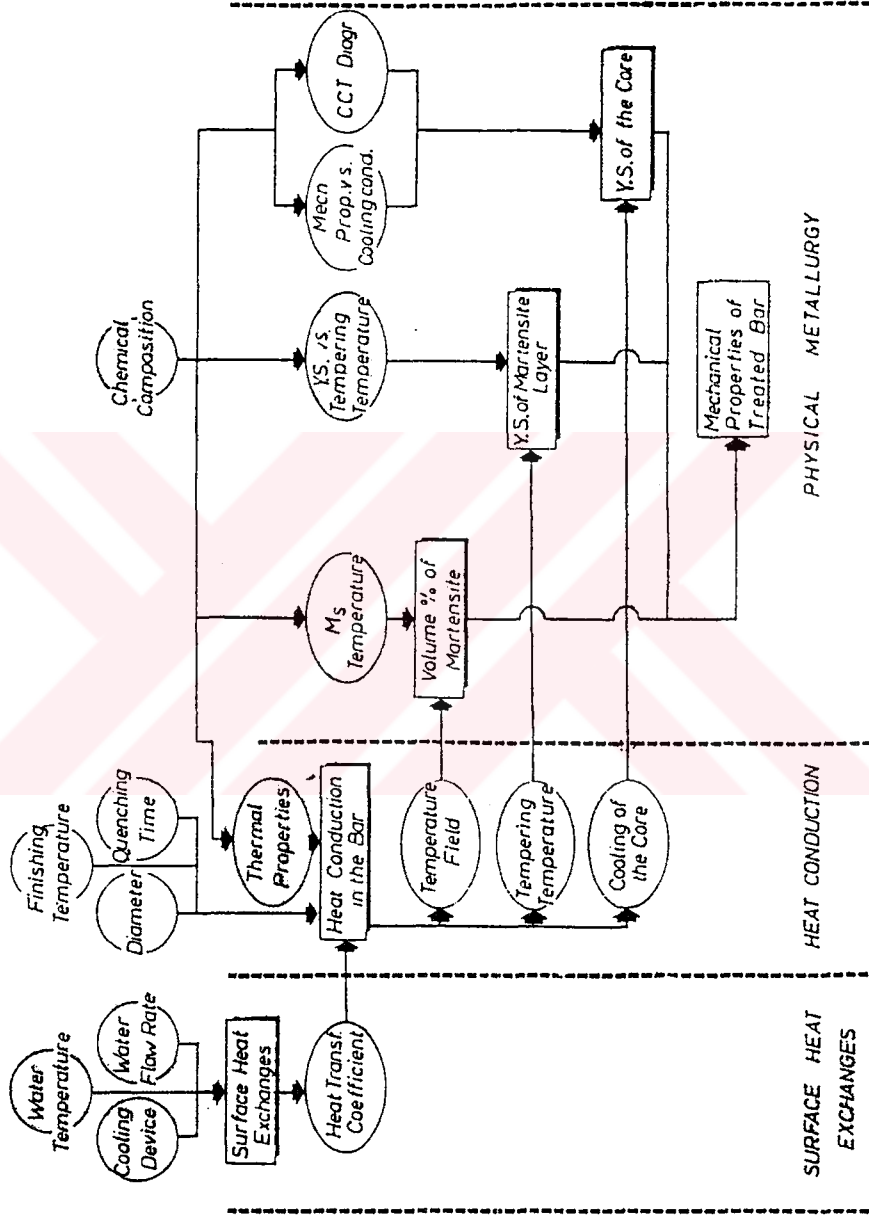
FIGURE 2.1 Fundamental Mechanisms of Tempcore Hardening

The overall macroscopic properties of the bar, particularly tensile properties, depend on three factors:

- the volume percentage of martensite ;

-the tensile properties of martensite ;

-the tensile properties of the core ferrite-carbides structure.

The volume percentage of martensite depends on the starting temperature of martensite transformation (M_s point), itself a function of composition and the temperature field in the cross-section of the bar leaving the quenching device. It is conventionally considered that the limit of the martensite layer corresponds to a circular cylinder of the same axis as the bar and for which the minimum temperature is equal to the M_s point.

The tensile properties of the martensitic layer depend on the chemical composition and on the "Tempering Temperature" defined in section 2.1.2 This tempering temperature is itself a function of the thermal field in the cross-section of the bar leaving the Tempcore cooling device.

The mechanical properties of the core depend on two groups of parameters :

-the chemical composition through CCT diagrams and microstructure -properties relations ;

-the cooling conditions during the quenching and the subsequent cooling stages.

It results from the above analysis that, for a given chemical composition, the main factor determining the mechanical properties of the bars is the thermal field resulting from the quenching stage. This thermal field is governed by the well known laws of conduction of heat in solids.

For a given bar diameter, the thermal field can be modified by changing the temperature of the bar entering the quenching device, the duration of the quenching stage and the heat transfer coefficient between the bar surface and the cooling water.

The heat transfer coefficient is the key factor of the Tempcore process ; it is expressed as a function of the surface temperature of the bar, function depending mainly on the design of the cooling device and the cooling water flow rate and temperature.

The above analysis shows that the hardening mechanism of Tempcore bars is an intricate one ; nevertheless, we shall show that, despite this fact, it is possible to find relatively simple relations describing the more important phenomena.

2.3 Surface Heat Exchanges

As far as surface heat exchanges are concerned, a Tempcore heat treating line can be divided in three sections : the drastic water quenching section, the air cooling section during the travel of the bar between the exit of the quenching line and the cooling bed, the air cooling of parallel bars lying on the cooling bed.

In order to describe the cooling on each of the above sections in a practical sense (i.e. disregarding the complicated fundamental mechanisms of cooling), we use the very convenient parameter called "Heat Transfer Coefficient" (α) and defined as follows :

$$\text{Heat Flux Density } (\varphi) = \alpha \, (T_s - T_m) \tag{2.1}$$

where T_s represents the surface temperature of the bar and

T_m the bulk temperature of the surrounding cooling medium.

In general, the heat transfer coefficient is very strongly dependent on the surface temperature and on the specific parameters of the cooling device considered.

Figure 2.2 shows a typical heat transfer coefficient - surface temperature curve.
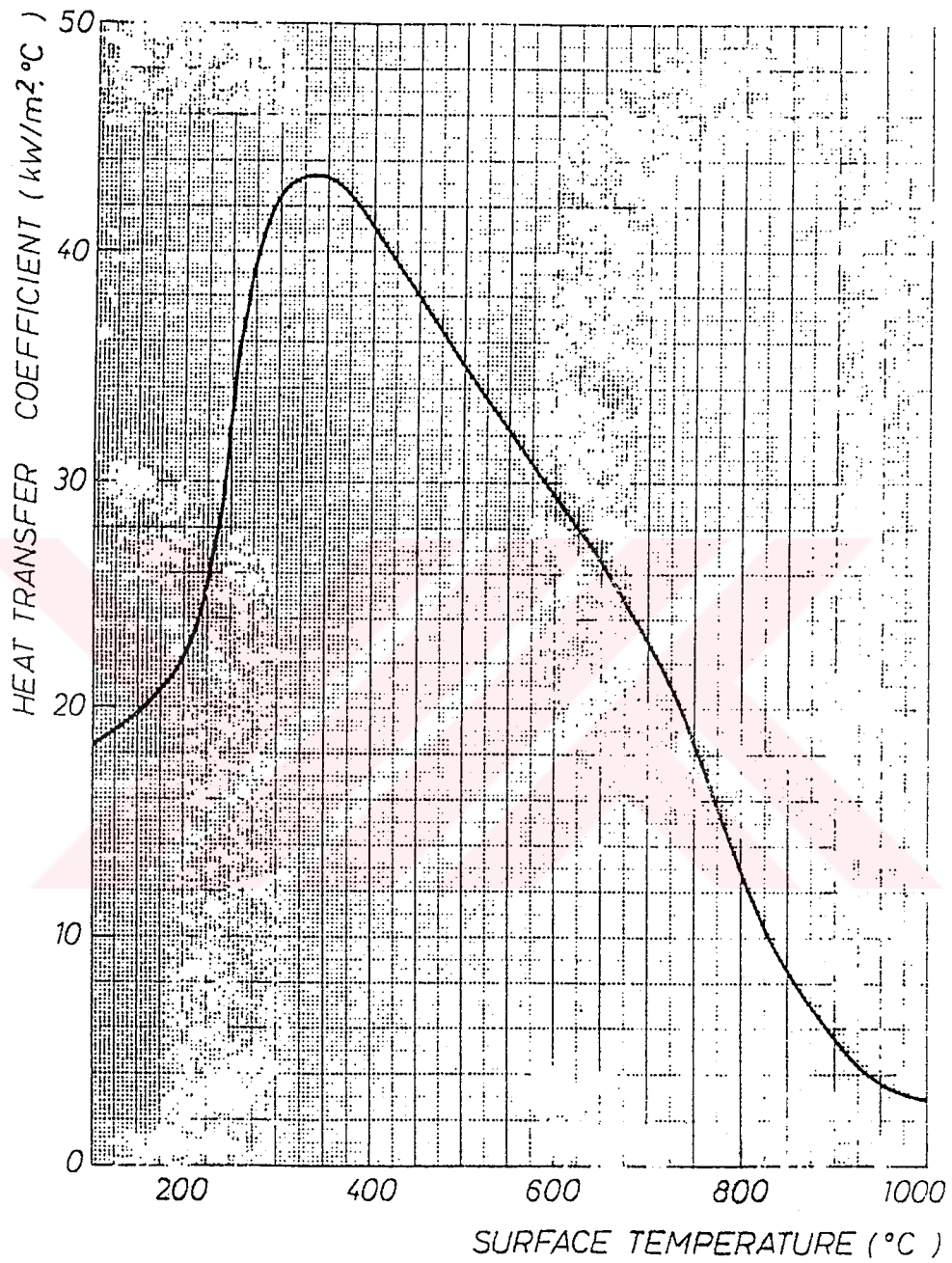
FIGURE 2.2 Heat Transfer Coefficient in a Tempcore Cooling Device

During the travel of the bar between the exit of the quenching line and the cooling bed, cooling results from a combination of radiation and forced air convection. The heat transfer coefficient is a function of the surface temperature of the bar and of the relative speed between the bar and the surrounding air.

The heat transfer coefficient on the cooling bed results from a combined radiation and natural convection cooling. Due to the view factor effect, the heat transfer coefficient depends not only on the surface temperature of the bar but also on the bar diameter and the distance between the notches of the cooling bed.

Table 2.1 shows the changing heat capacity and heat conduction coefficient as a function of internal structure and temperature. Changing internal structure and temperature change heat capacity and heat conduction coefficient.

Table 2.1 Heat Capacity and Heat Conduction Coefficient (CRM, 1985)

Temperature	Structure	0 ^{0}C	300 ^{0}C	600 ^{0}C	900 ^{0}C
Conduction Coefficient k (cal/mm.sec^{0}C)	γ	0.004	0.005	0.006	0.007
	α, p, b, m	0.013	0.0105	0.009	0.007
Heat Capacity ρ c_p (cal./mm^3 ^{0}C)	γ	0.00076	0.00086	0.00095	0.00105
	α, p, b, m	0.00084	0.00092	0.00102	0.00110

2.4 Heat Conduction in the Bar

It has been shown in section 2.2 that, for a given chemical composition, the final tensile properties of a Tempcore treated bar depend exclusively on the thermal field in the bar at the moment it leaves the quenching devices. In the following paragraphs, the dependence of the thermal field on the different process parameters will be discussed in more details.

As a first step, the problem of heat conduction in the bar has to be solved ; its solutions requires :
- the definition of the boundary conditions. The knowledge of the heat transfer coefficients presented in the previous paragraph constitutes a satisfactory definition of these boundary conditions ;

- the knowledge of the thermal properties of the steel. Temperature dependent properties gathered from technical literature are used ;

- the numerical solutions of the Fourier differential equation and its implementation in a computer program.

The solution of the heat conduction problem enables the calculation of the temperature at any moment and any point of the cross-section of the bar. Having thus determined the thermal field in the bar, it is possible to calculate the two important parameters from a metallurgical point of view : the volume percentage of martensite (p_m) and the "theoretical tempering temperature" (T^*) defined below.

The following sections will be devoted to the study of the effect of quenching conditions on (p_m) and (T^*).

2.4.1 Volume Percentage of Martensite

Figure 2.3 shows the temperature distribution in the cross-section of a 25 mm diameter bar after 1, 1.5 and 2 seconds quenching.

It is interesting to observe the very steep temperature gradient near the surface ; this is an important characteristic of the Tempcore quenching equipment because it enables to form a relatively thick layer of martensite and, in the same time, to leave enough heat in the core for the self-tempering operation.
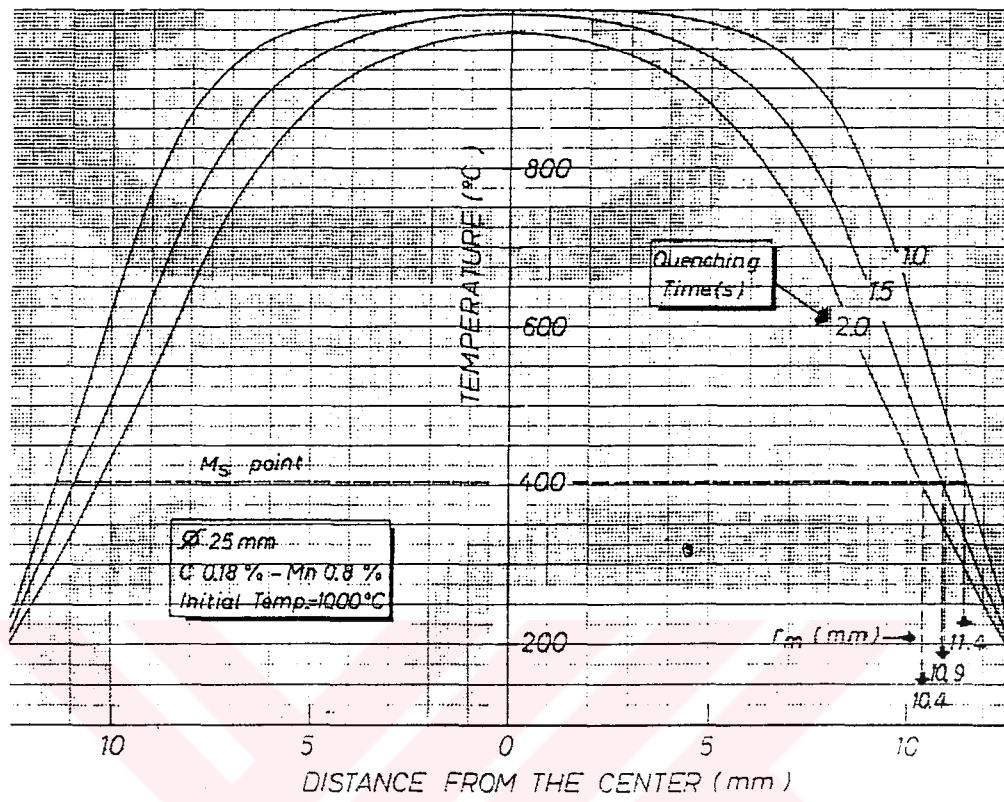
Figure 2.3 Temperature Distribution in a 25 mm. Φ Bar after Quenching.

For each of the three quenching times, Figure 2.3 shows the radius limiting the martensitic layer (r_m) (according to the conventional definition of the section 2.2).

The starting temperature of the martensitic transformation (M_s) is a function of chemical composition. The following formula is sufficient for our study :

$$M_s = -361 \, (C\%) - 39 \, (Mn \, \%) + 500 \qquad (2.2)$$

If (d) represents the equivalent diameter of the bar, the volume percentage of martensite is expressed by the relation :

$$P_m = 100 \left[1 - \left(\frac{2 \, r_m}{d} \right)^2 \right] \qquad (2.3)$$

In the example of Figure 2.3. : p_m = 30.8 %, 24.3 % and 16.8 % for the quenching times of 2 sec., 1.5 sec. and 1 sec. respectively.

For a given cooling device, water flow rate per unit length and water temperature, and for a fixed chemical composition, the percentage of martensite is a function of the quenching time, the diameter of the bar and its entry temperature in the quenching device.

The relation p_m - quenching time can be considered with a very good approximation as linear (Fig. 2.4) in the useful range of (p_m) (CRM, 1985). The slope of this curve increases sharply with decreasing diameters. We shall show later that this rapid increase of the slope does not create any problem as far as the controllability of the process is concerned.

Figure 2.4 shows also (compare lines c and d) the effect of the initial quenching temperature: the slope of the "p_m - time" line is not affected but (p_m) significantly decreases when (T_0) increases. This fact has to be kept in mind when discussing the effect of thermomechanical treatment (section 2.3).
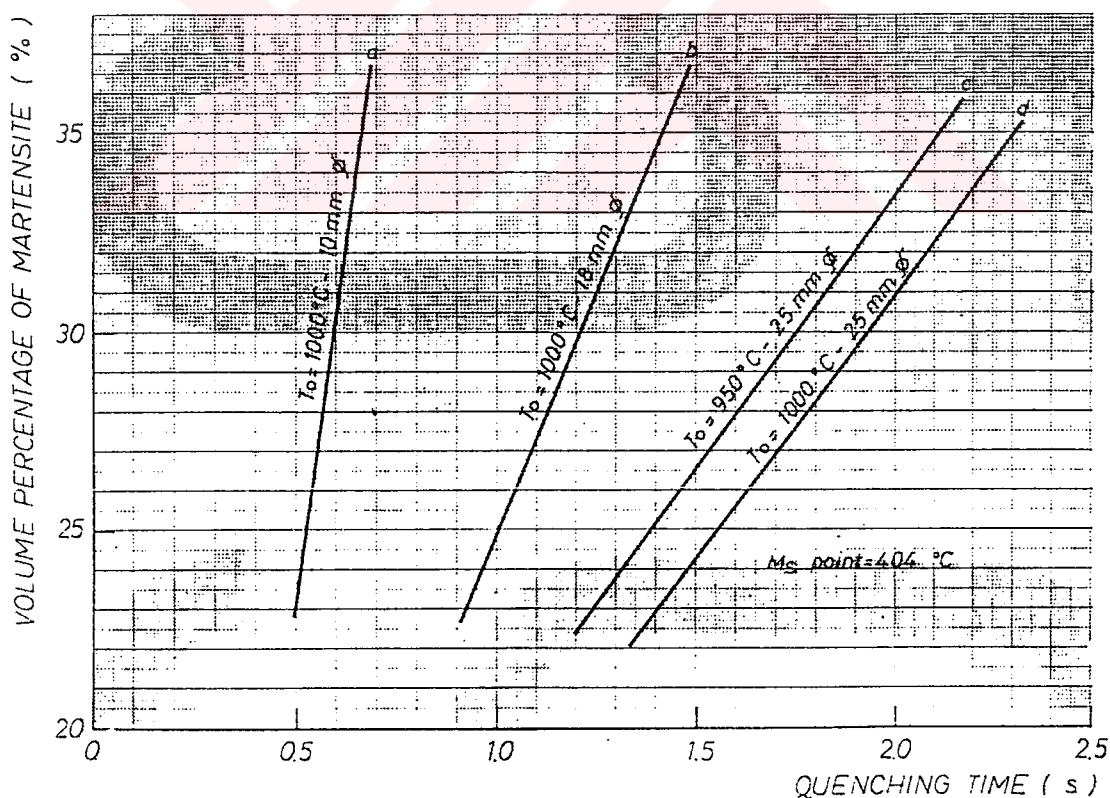
Figure 2.4 Effect of Quenching Time, Bar Diameter and Initial Temperature on the Martensite Content.

2.4.2 Tempering Temperature

The tempering temperature has been defined in section 2.1 as being the maximum temperature reached at the surface of the bar during the self-tempering stage. This parameter (T_r) is important in practice for two reasons :

-it corresponds to the minimum tempering temperature of the martensitic surface layer ;

-it can be measured directly by a radiation pyrometer and be used for controlling the process (section 2.6)

From the point of view of the theoretical analysis of the process, we shall use another parameter called "theoretical tempering temperature", symbolized by (T^*) and corresponding to the following definition : let it be the enthalpy per unit length of the bar at the exit of the quenching device ; (T^*) is the uniform temperature of a bar in all respects identical to the considered one and having the same enthalpy per unit length.

The interest of (T^*) is that its value is exclusively linked to the temperature field at the exit of the quenching device : the phenomena occurring during the air cooling phase have not to be taken into account.

The difference $(T^* - T_r)$ depends on the heat transfer coefficient in the forced air cooling section and on the time necessary for the surface of the bar to reach (T_r). As this time increases with the bar diameter, so does the difference $(T^* - T_r)$ (fig. 2.5).

With the above remarks in mind, one can now discuss the effect on (T^*) of the bar diameter (d), the initial temperature (T_0) and the quenching time (t).
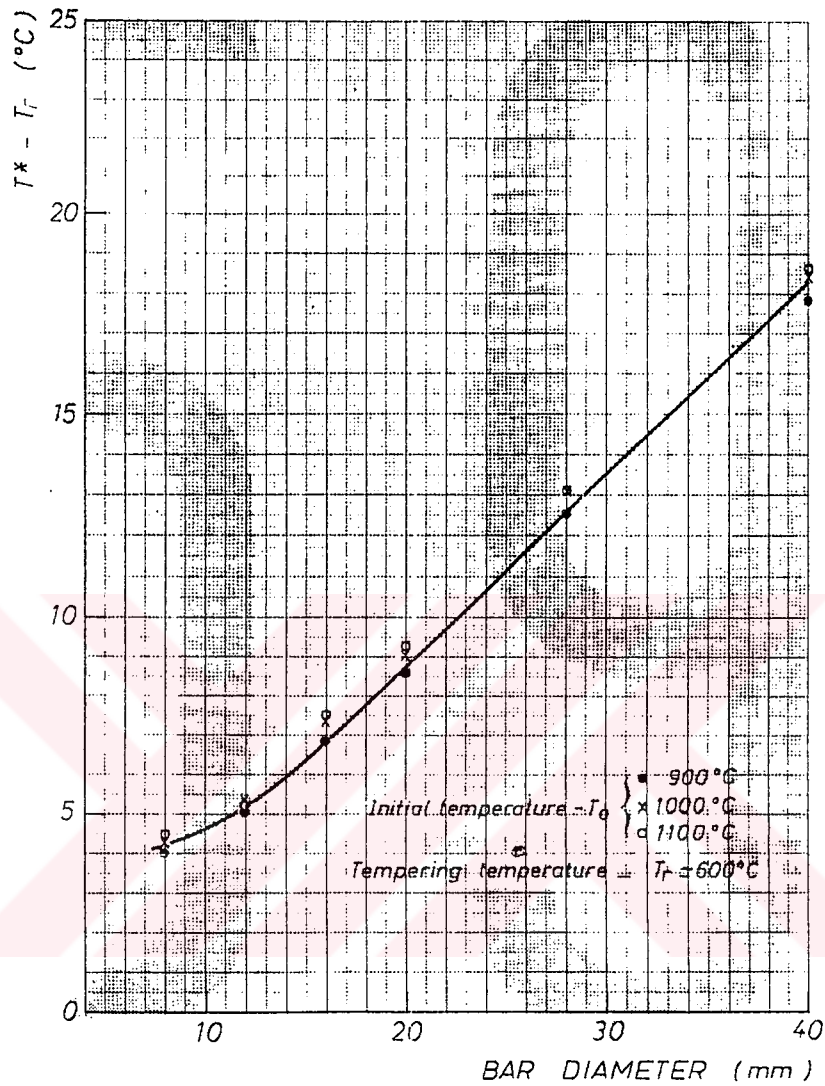
Figure 2.5 Difference (T*-T$_r$) as a Function of the Bar Diameter.

Figure 2.6 shows that the relation T* (t) is linear and that the slope $\left(\dfrac{dT^*}{dt}\right)$ is strongly dependent on the diameter (CRM,1985). The initial temperature has only a translation effect on T* (t). The relation between the above parameters can be expressed analytically by :

$$T^* = - A\, d^{-\beta}\, t + f(T_0,d) \tag{2.4}$$

in which A and β are constants.
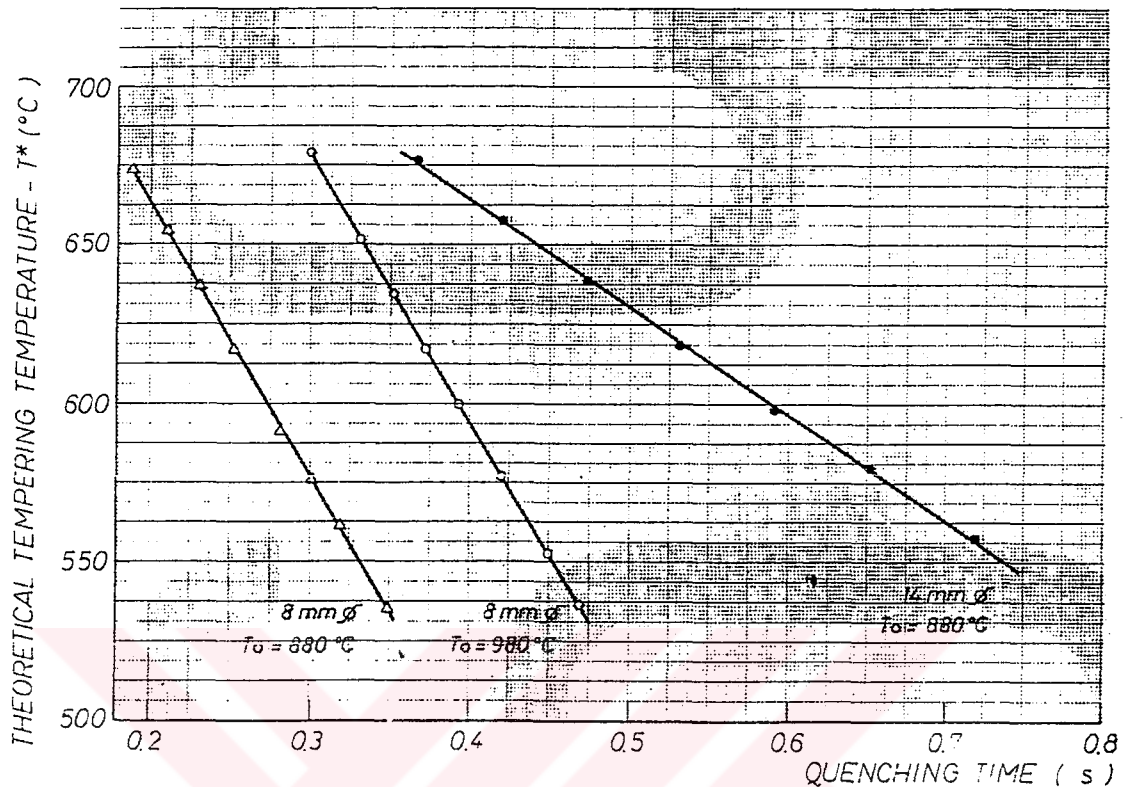
Figure 2.6 Effect of Diameter, Initial Temperature and Quenching Time on the Theoritical Tempering Temperature.

2.4.3 Control Function of the Process

As (T_r) and (p_m) are the main controlling factors of the tensile properties, it is interesting to establish a relation between them.

Figure 2.7 shows that the relation "p_m - (T_r)" is linear and that the slope $\left(\dfrac{dP_m}{dt} \right)$ is approximately independent on the bar diameter (CRM, 1985). With increasing diameters, the "p_m - (T_r)" line undergoes a parallel translation towards increasing tempering temperatures. For practical applications, a single "p_m - (T_r)" relation can be considered for diameters between 16 mm and 40 mm.

The effect of initial quenching temperature on the relation "p_m - (T_r)" is shown by figure 2.8 (CRM, 1985). In practice and for normal operating conditions, the variation of finishing temperature for the same diameter does not exceed + 50 ^{0}C. The same maximum range of variation can be foreseen for (T_0). In that case, we can neglect, for practical purposes, the influence of entry temperature on the relation "p_m - (T_r)".
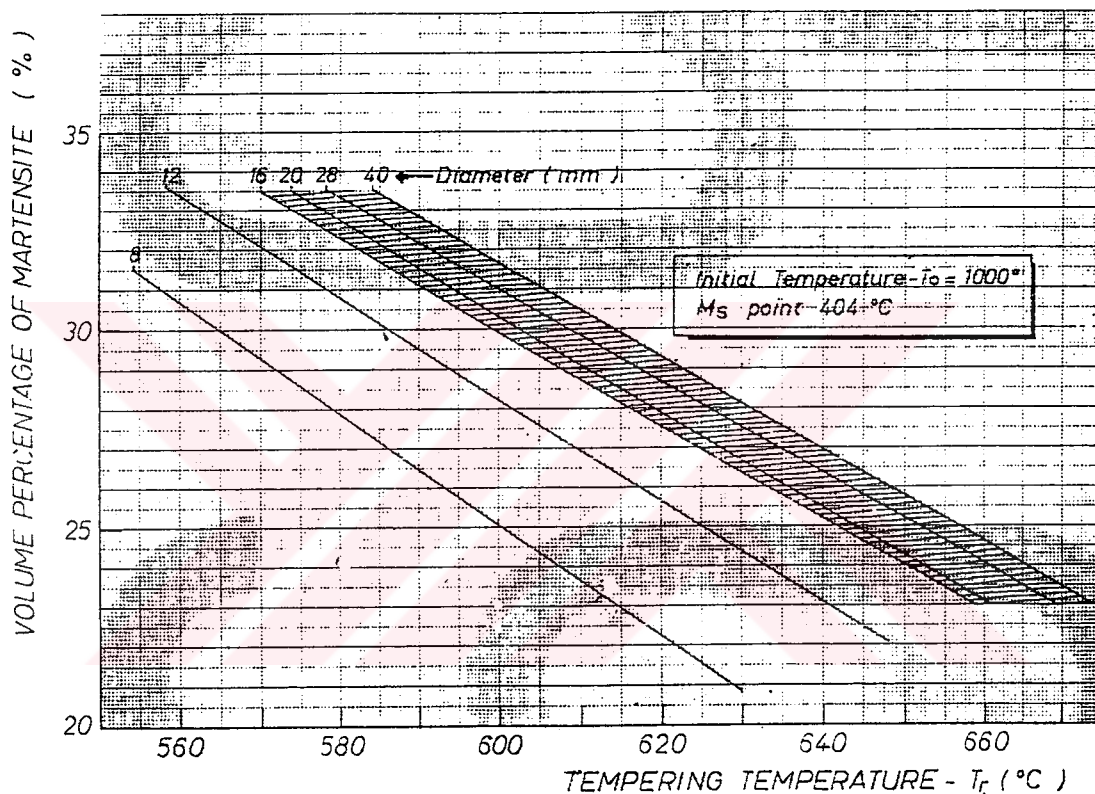
Figure 2.7 Effect of Bar Diameter on the p_m (T_r) Relation.

From the above analysis, one can conclude that to each pair (d - T_0) corresponds a relation p_m - (T_r) that will be used to control the process. For $16 \le d \le 40$ mm, a single relation can be defined.
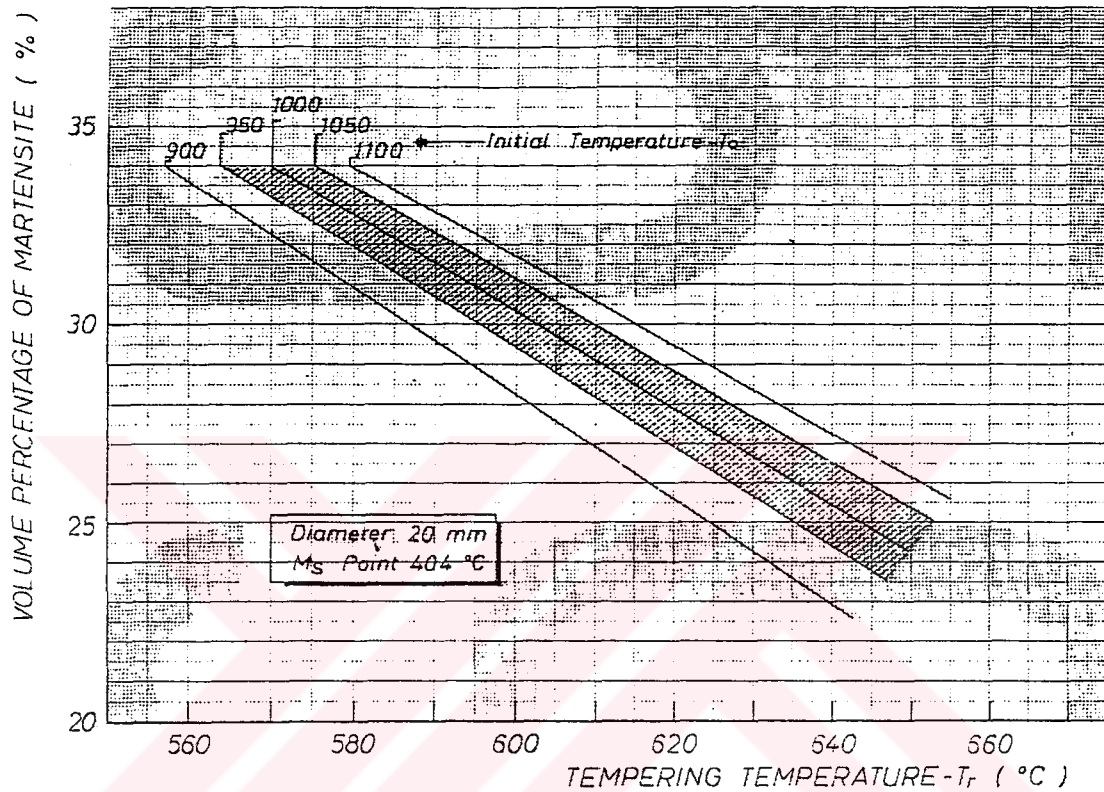
Figure 2.8 Effect of Initial Temperature on the p_m (T_r) Relation.

2.5 Mechanical Properties

In the previous sections, the effect of the independent variables of the process on two important parameters has been discussed: the volume percentage of martensite (p_m) and tempering temperature (T^* or T_r).

In this section, (p_m) and (T_r) will be considered as the independent variables and their effects on mechanical properties will be discussed. As metallurgical phenomena are

involved, an additional important variable will be introduced : chemical composition. For the steel grades treated by the Tempcore process, carbon and manganese (in some cases silicon) contents are the main components characterizing the composition from a practical point of view.

In two separate sections the properties of the tempered martensite and those of the core of the treated bars will be discussed. In a third section, the combination of the two individual zones of the bar leading to the final properties, will be discussed.

2.5.1 Tempered Martensite

The properties of tempered martensite depend exclusively on its composition and on the tempering temperature. In order to determine these relations in this case of Tempcore steels, specimens of different compositions have been quenched in still water and submitted to a subsequent tempering treatment (CRM,1985).

The following relation gives the yield strength (expressed in MPa) of the martensitic layer with a precision sufficient for practical uses :

$$Y_m = -1.75 \ T_r + 1781.5 \qquad (2.5)$$

2.5.2 Central Region of the Bar

One calls "central region of the bar" or "core" the part of the bar in which the temperature at the exit of the quenching line is higher than the M_s temperature. It is obvious that at each point of the cross section corresponding to the core, the cooling curve and, consequently, the properties are different. This situation being too complicated to be handled by simple analysis, it has been simplified drastically in this section.

The observation of Figure 2.9 suggests a stylization of the mean cooling curve of the core (CRM, 1985).

The cooling of the core can be assimilated roughly to an isothermal transformation at temperature T_c
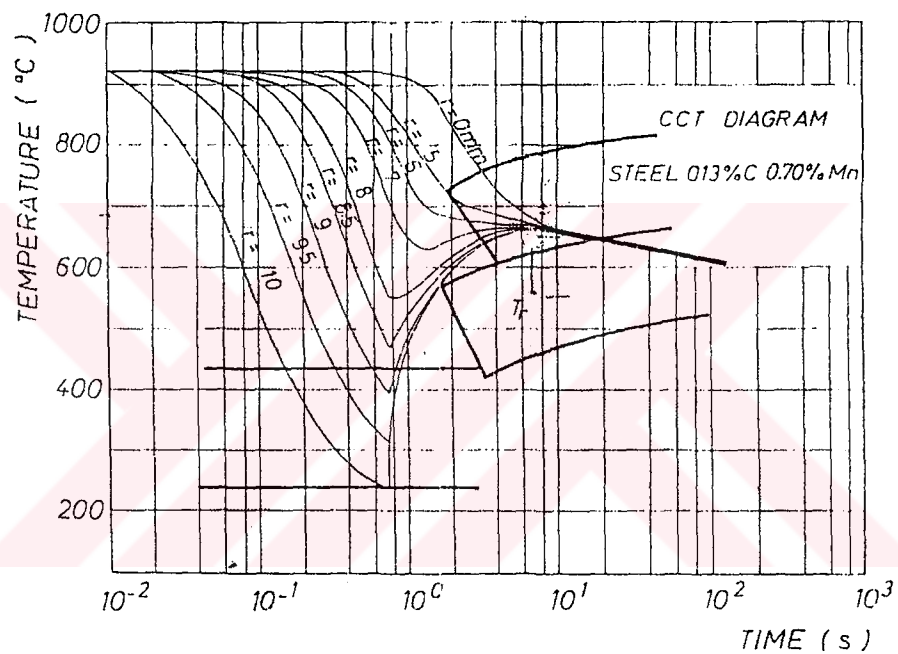

Figure 2.9 Temperature Time Curves in a 20 mm. Φ Bar Treated According to the Tempcore Process.

In order to determine the relation between the yield strength of the core (Y_c) and (T_c) and the composition, some treated specimens of the steels are listed in table 2.1. by austenizing and quenching in a lead bath at different temperatures (T_c) (CRM, 1985).

Table 2.2 - Isothermal Treatments in Pb Bath

Composition (%)				Y_c (Mpa) for T_c (°C)				
C	Mn	Si	N_2	550	575	600	625	650
0.139	0.64	0.037	0.014	365	354	340	334	318
0.120	0.59	0.025	0.012	340	330	317	309	298
0.211	0.79	0.005	0.001	371	357	354	351	349
0.112	0.93	0.026	0.004	335	317	310	304	301
0.199	0.875	0.005	0.009	380	362	356	352	347
0.130	1.213	0.03	0.013	402	384	366	350	330
0.148	0.955	0.024	0.004	337	324	313	304	294

A regression analysis of the results given in table 2.1. leads to the following formula :

$$Y_c = - 0.406 \ T_c + 357 \ (C \ \%) + 38.7 \ (Mn \ \%) + 495 \qquad (2.6)$$

The observation of Fig.2.9 shows that, at first approximation, the value of (T_c) in the above formula can be taken equal to (T_r).

2.5.3 Overall Yield Strength of the Tempcore Bar

Having determined the yield strength of the two regions into which the cross-section of a Tempcore bar has been artificially divided, one seeks a way to combine (Y_m) and (Y_c) in order to foresee the overall yield strength of the bar.

Let us think of a Tempcore bar as being divided in a series of concentric tubes, the mechanical properties varying from one tube to the other.

As there is a continuity between a tube and its neighbours the problem consisting to calculate the overall properties knowing the individual properties of the tubes, is a complicated one.

Two important simplifications, justified by experimental evidence, will be introduced :

a) additivity of the tensile forces. This hypothesis has been verified with a reasonable precision by tensile tests on Tempcore bars machined at progressively smaller diameters and also on tubes machined by boring bars to progressively higher diameters :

b) the continuous variation of properties is neglected and only two zones are considered : a surface layer having a yield strength (Y_m) and occupying (p_m)% of the volume and a core zone with a yield strength (Y_c) and occupying ($1 - p_m$) % of the volume.

It is easy to demonstrate that under the above conditions :

$$Y = p_m Y_m + (1 - p_m) Y_c \qquad (2.7)$$

Finally, the Tempcore process is described by the following relations :

$$p_m = f(t, d, T_0, M_s) \qquad (2.8)$$

$$T_r = f(t, d, T_0) \qquad (2.9)$$

$$M_s = -361 C - 39 Mn + 500 \qquad (2.10)$$

$$Y_m = -1.75 T_r + 1781.5 \qquad (2.11)$$

$$Y_c = -0.406 T_r + 357 C + 38.7 Mn + 495 \qquad (2.12)$$

$$Y = p_m (Y_m - Y_c) + Y_c \qquad (2.13)$$

2.6 Practical Conclusions of the Theoretical Study

The mathematical model represented by relations 2.8 to 2.13 will now be used in order to derive some interesting practical conclusions.

Let us consider a typical Tempcore steel containing 0.18 % C and 0.8 % Mn. The relations (2.8) to (2.13) can be combined in the following formula :

$$Y = p_m (1191 - 1.344 \ T_r) - 0.406 \ T_r + 590 \qquad (2.14)$$

By using equation (2.14) and the results presented in section 2.4., we can establish a relation between the yield strength of the bar and the tempering temperature.

CHAPTER THREE
HEAT TRANSFER AND FINITE ELEMENTS
MODELING

3.1 Introduction

Heat transfer analysts often calculate temperature distributions as a first step in the selection of materials or for the design of structures that may experience abnormal temperature levels during their service life. Analysts must be able to model realistically environmental boundary conditions, represent complicated geometry, and analyze a variety of materials that deviate from simple constant-property isotropic materials. Textbook problems often assume away these realistic challenges. Because finite difference approaches seldom meet these challenges adequately, there is an increasing interest in finite element methods (Huebner, 1982).

Finite element researchers in the late 1960s sometimes regarded heat transfer analysis as simply a special example of a field problem. Often this view was understandable, because many of the early finite element researchers had structural backgrounds and failed to appreciate the subtleties of thermal-fluid analysis.

We present a finite element formulation for computation of the steady-state temperature distribution $T(r,z)$ for solids with general surface heat transfer.

3.2 Problem Statement

Consider steady-state heat transfer in a two-dimensional isotropic solid Ω bounded by a surface Γ (Figure 3.1). The problem is governed by the energy equation.

$$-\left(\frac{\partial q_r}{\partial r} + \frac{\partial q_z}{\partial z}\right) = \rho c_p \frac{\partial T}{\partial t} \tag{3.1}$$

where q_r and q_z are components of the heat flow rate vector per unit area in polar coordinates (r,z), ρ is density, and c_p is the specific heat.

Figure 3.1 Two-dimensional solution domain for heat conduction.

Heat conduction boundary conditions take several forms considering the frequently encountered conditions of specified surface temperature and specified surface heat. The boundary conditions (Figure 3.1) are

$$T_s = T_1 (r,z,t) \qquad \text{on } S_1$$

$$\tag{3.2}$$

$$q_r n_r + q_z n_z = h (T_s - T_e) \qquad \text{on } S_2$$

where T_1 is the specified surface temperature, which may vary with time, n_r and n_z are the direction cosines of the outward normal to the surface, h is a convective heat transfer coefficient that may be a function of the convective exchange temperature T_e and/or time, T_s is the unknown surface temperature.

Isotropic medium Fourier's law is,

$$q_r = -k\frac{\partial T}{\partial r}$$

$$(3.3)$$

$$q_z = -k\frac{\partial T}{\partial z}$$

From (3.3.) $q_r \neq q_z$ $\qquad$ (3.4)

The initial condition specifies the temperature distribution at time zero,

$$T(r,z,0) = T_0 (r,z) \qquad (3.5)$$

3.3 Finite Element Formulation

The solution domain V is divided M elements of k nodes each. By the usual procedure the temperature gradients for each element can be expressed as

$$T^{(e)}(r,z,t) = \sum_{i=1}^{k} N_i(r,z)T_i(t) \qquad (3.6)$$

$$\frac{\partial T^{(e)}}{\partial r}(r,z,t) = \sum_{i=1}^{k} \frac{\partial N_i}{\partial r}(r,z)T_i(t)$$

$$(3.7)$$

$$\frac{\partial T^{(e)}}{\partial z}(r,z,t) = \sum_{i=1}^{k} \frac{\partial N_i}{\partial z}(r,z)T_i(t)$$

or in matrix notation

$$T^{(e)}(r,z,t) = [N(r,z)]\{T(t)\} \tag{3.8}$$

$$\left\{\begin{array}{c} \dfrac{\partial T}{\partial r}(r,z,t) \\[2ex] \dfrac{\partial T}{\partial z}(r,z,t) \end{array}\right\} = [B(r,z)]\{T(t)\} \tag{3.9}$$

where $[N]$ is the temperature interpolation matrix, $[B]$ is the temperature-gradient interpolation matrix.

$$[N(r,z)] = [N_1 N_2 \ldots\ldots\ldots N_k] \tag{3.10}$$

$$[B(r,z)] = \begin{bmatrix} \dfrac{\partial N_1}{\partial r} & \dfrac{\partial N_2}{\partial r} & \cdots\cdots & \dfrac{\partial N_k}{\partial r} \\[2ex] \dfrac{\partial N_1}{\partial z} & \dfrac{\partial N_2}{\partial z} & \cdots\cdots & \dfrac{\partial N_k}{\partial z} \end{bmatrix} \tag{3.11}$$

$T_i(t)$ is the value of the temperature at each node and $\{T(t)\}$ is the vector of element nodal temperatures. The second-order heat conduction equation requires only C^0 continuity, and we may use temperature as the only nodal unknown.

The method of weighted residuals requires.

$$\int_{V^{(e)}} \left(\frac{\partial q_r}{\partial r} + \frac{\partial q_z}{\partial z} + \rho c_p \frac{\partial T}{\partial t}\right) N_i \, dV = 0 \tag{3.12}$$

Where $V^{(e)}$ is the domain for element (e). We integrate the term.

$$\int_{V^{(e)}} \left(\frac{\partial q_r}{\partial r} + \frac{\partial q_z}{\partial z}\right) N_i \, dV \tag{3.13}$$

by Gauss's theorem, which introduces surface integrals of the heat flow across the element boundary $\Gamma^{(e)}$. We write the result in the rearranged form.

$$\int_{V^{(e)}} \rho c_p \frac{\partial T}{\partial t} N_i dV - \int_{V^{(e)}} \left[\frac{\partial N_i}{\partial r} \frac{\partial N_i}{\partial z} \right] \left\{ \begin{matrix} q_r \\ q_z \end{matrix} \right\} dV = -\int_{\Gamma^{(e)}} (q.n) N_i d\Gamma$$

(3.14)

$$i = 1, 2, \ldots\ldots k$$

Next we express the surface integral as the sum of the integrals over. S_1 and S_2 introduce the boundary conditions, equations (3.2) and (3.3). Thus

$$\int_{V^{(e)}} \rho c_p \frac{\partial T}{\partial t} N_i dV - \int_{V^{(e)}} \left[\frac{\partial N_i}{\partial r} \frac{\partial N_i}{\partial z} \right] \left\{ \begin{matrix} q_r \\ q_z \end{matrix} \right\} dV =$$

$$-\int_{S_1} (q.n) N_i d\Gamma - \int_{S_2} h(T - T_e) N_i d\Gamma$$

(3.15)

For convience we first write equation (3.3) in matrix form,

$$\left\{ \begin{matrix} q_r \\ q_z \end{matrix} \right\} = -k \left[\begin{matrix} \dfrac{\partial T}{\partial r} \\ \dfrac{\partial T}{\partial z} \end{matrix} \right]$$

(3.16)

Where k is the thermal conductivity, and then express the temperature gradients in terms of the nodal temperatures through equation (3.11):

$$\left\{ \begin{matrix} q_r \\ q_z \end{matrix} \right\} = -k[B]\{T\}$$

(3.17)

Finally, after some manipulation the resulting element equations become

$$[C] \frac{\partial T}{\partial t} + \left[[K_c] + [K_h] \right] \{T\} = \{R_h\}$$

(3.18)

$$\frac{\partial T}{\partial t} = \frac{T_{n+1} - T_n}{\Delta t} \qquad (3.19)$$

so

$$[C]\{T_{n+1}\} = \{R_h\}\Delta t - [[K_c] + [K_h]]\Delta t.\{T_n\} + [C]\{T_n\} \qquad (3.20)$$

$$\{T_{n+1}\} = [C]^{-1}\{\{R_h\}\Delta t + [C]\{T_n\} - [[K_c] + [K_h]]\Delta t\{T_n\}\}$$

where,

$$[C] = \int_{V^{(e)}} \rho c_p [N]^T [N] dV \qquad (3.21)$$

$$[K_c] = \int_{V^{(e)}} k [B]^T [B] dV \qquad (3.22)$$

$$[K_h] = \int_{S_2} h [N]^T [N] d\Gamma \qquad (3.23)$$

$$\{R_h\} = \int_{S_2} h T_e \{N\} d\Gamma \qquad (3.24)$$

The coefficient matrix $[C]$ of the time derivative of the nodal temperatures is the element capacitance matrix. The coefficient matrices $[K_c]$ and $[K_h]$ are element conductance matrices and relate to conduction and convection, respectively. The convection is computed only for elements with surface convection. The vector $\{R_h\}$ is surface convection.
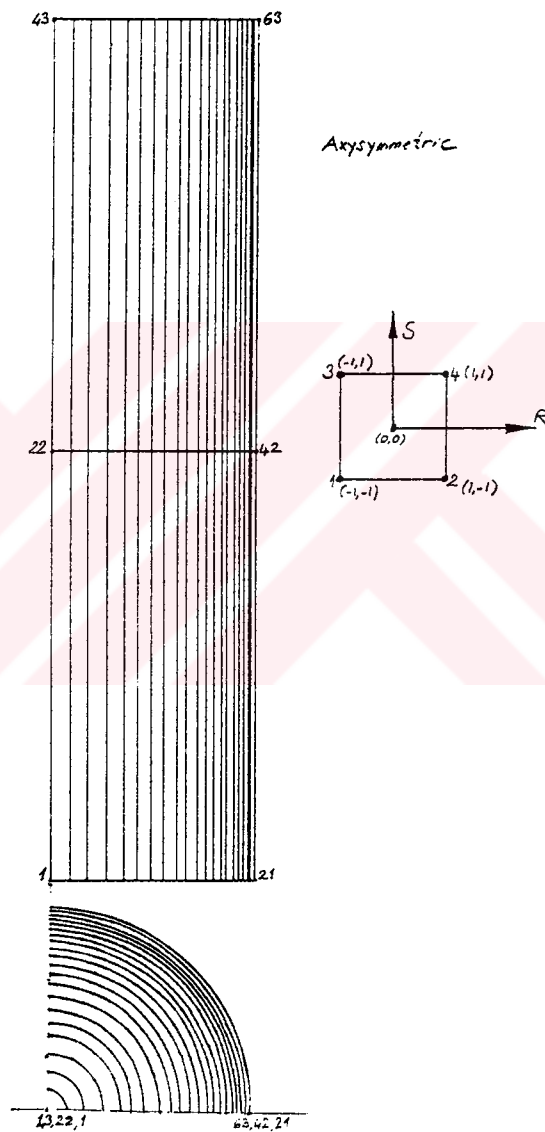
Figure 3.2 The Finite Element Model of Cylindrical Shape

CHAPTER FOUR

TRANSITION FROM ISOTHERMIC TTT TO CONTINUOUS COOLING TRANSFORMATION (CCT) CURVES

4.1 Pearlitic and Bainitic Transformation

It is possible to obtain continuous cooling curves from isothermic time temperature transformation (TTT) diagrams. Firstly, we need some fundamental relations for this procedure.

The amount of isothermic transformation can be given by the relation (4.1) (Yu, 1977)

$$W(t,T) = 1-\exp.(-bt^n) \qquad (4.1)$$

where,

W: the weight ratio of the transformed phase

b, n: the coefficients changing by temperature

If austenite (γ) transforms to ferrite (α) and pearlite then $W=W_{F/P}$. If austenite transforms to bainite then $W=W_B$. The curves in the figure 4.1 are also separated into two different regions as pearlitic (or pearlitic + ferritic) and bainitic regions. In order to calculate the ratio of the transformations, b and n should be determined. They depend on temperature

$$\log b = c_{b0} + c_{b1}T + c_{b2}T^2 + c_{b3}T^3$$

$$(4.2)$$

$$n = c_{n0} + c_{n1}T + c_{n2}T^2 + c_{n3}T^3$$

where c_{bi} and c_{ni} are constants. These constants for two regions above are obtained as follows: The first curve on the figure 4.1 is transformation start curve and expresses 1 percent transformation. Second curve is transformation finish curve and expresses 99 percent transformation. If we want to calculate eight constants given in equation (4.2) for the transformation from austenite to pearlite we must select four different temperatures over the bend of the S curve (Fig.4.1). We obtain eight equations from (4.1) and (4.2) and determine eight constants.
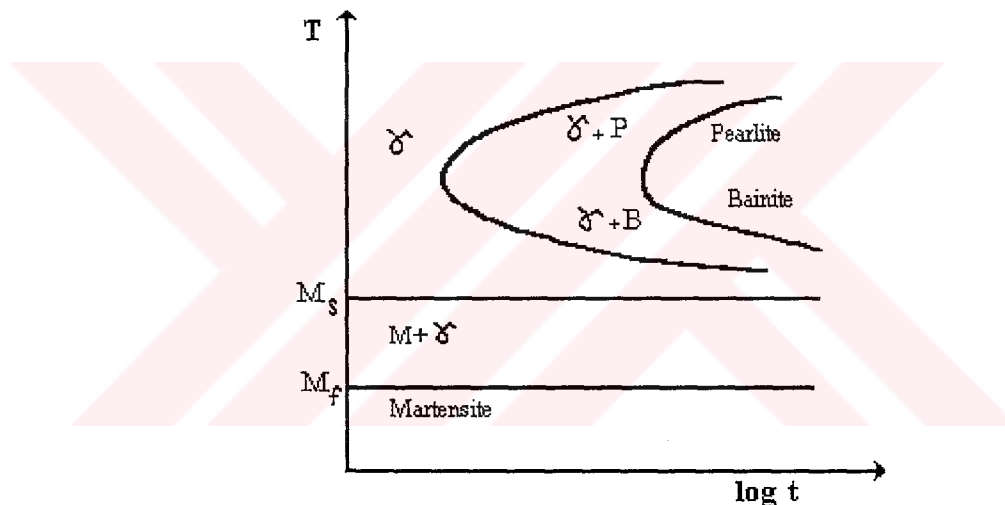
Figure 4.1 Isothermal TTT

Same procedure is applied for the bainitic region, so the constants of this region are also determined. Thus, each phase and the amount of this phase at any temperature and any time are determined by using (4.1) and (4.2) equations. However, by these procedures we determine phase at the isothermic TTT diagram, we have to determine the amount of the phases by using continuous cooling curve because temperature decreases during the process in our study. Using some methods, the amount of the transformed phases during the continuous cooling can be determined from TTT curves. On this occasion, cooling curve is converted to step form, so curve is consist of to many isothermic steps. The total amount of the transformations at these isothermic steps gives the amount of phases that occur as a

result of continuous cooling (Fig. 4.2). Naturally, if the intervals of temperature and time become smaller, the sensitivity of the calculation increases.
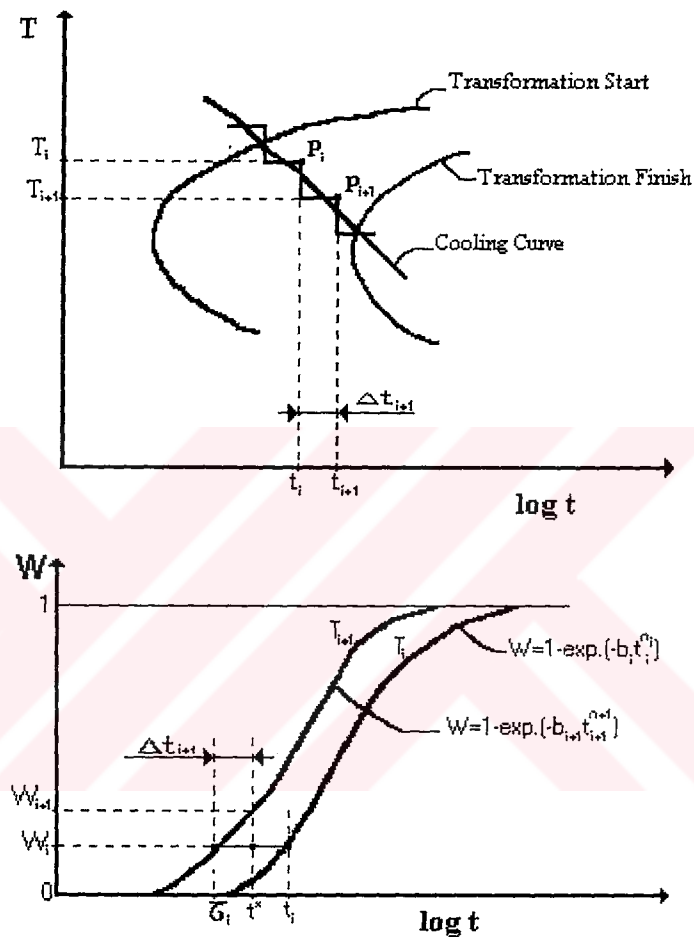
Figure 4.2 Isothermal Steps

Let the transformation start at the T_i temperature step, the amount of transformation at P_i point can be expressed as

$$W_i = 1 - \exp.(-b_i t_i^{ni}) \qquad (4.3)$$

At the continuous cooling state, t_{i+1} duration time is not valid for T_{i+1} temperature so we write a fictive waiting time.

$$t^* = \tau_i + \Delta t_{i+1} \tag{4.4}$$

where τ_i value is the time necessary for W_i transformation quantity to occur at the T_{i+1} temperature. Δt_{i+1} is the real waiting time at the T_{i+1} temperature. τ_i value is determined from equation (4.1) and (4.2) by using W_i, b_{i+1} and n_{i+1} values.

Consequently, the equation giving the amount of transformation for P_{i+1} point at temperature T_{i+1} is:

$$W_{i+1} = 1\text{-exp.}\left(-b_{i+1} t^{*n_{i+1}}\right) \tag{4.5}$$

That is to say, the ratio of the transformation for the point P_{i+1} is determined. This procedure is applied between transformation start and transformation finish curves.

4.2 Martensitic Transformation

Martensitic transformation does not depend on time but on temperature because there is no diffusion in martensitic transformation. It can be seen at isothermic TTT diagram. Martensitic transformation begins at $T=M_s$ and finishes at $T=M_f$. That is to say, if T is smaller than M_f there will be no austenite in the structure and all of the austenite transforms to martensite. Martensite quantity is given by the parabolic equation:

$$W_m = W^*\left\{1 - \left[\left(T - M_f\right) / \left(M_s - M_f\right)\right]^2\right\}$$

$$\tag{4.6}$$

$$W^* = 1 - \left(W_{F/P} + W_B\right)$$

where,

$W_{F/P}$: pearlite + ferrite ratio

W_B : bainite ratio
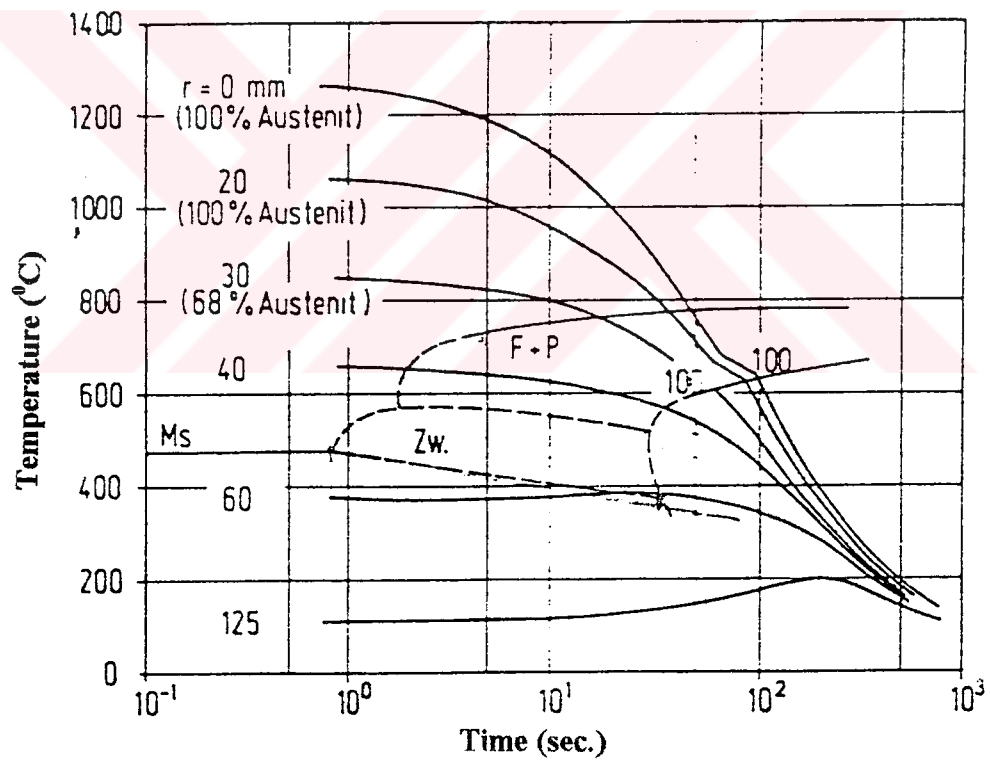
Figure 4.3 TTT Diagram of the St37 Steel

CHAPTER FIVE

EXPERIMENTS, CALCULATIONS AND RESULTS

5.1 Experimental Study and Results

5.1.1 Specimens

In experimental study, materials having chemical composition of %0.16-0.21C, %0.17-0.22Si, %0.74-0.83Mn has been used. Tempcore process has been applied to the products having 16, 18, 20, 22 mm. Φ notched bars. Tensile tests have been made in Alça having 60 ton capacity and Dartec having 120 kN. capacity tensile test machines. Polishing of specimens has been made by Distocom-2 and Struers apparatus. Experimental study has been carried out by L. Özsoyeller (Özsoyeller,1993) in the laboratory of İ.D.Ç. San. A. Ş.

5.1.2 Metallographic Inspection

Specimens, which have been taken from bars produced by Tempcore process, have been cut as 12 mm. length and put into polyester then specimens have been atched with 3 percent nital solution. Figure 5.1 shows the structures of steel bars with 18 mm. bar diameter depending on different quenching durations.
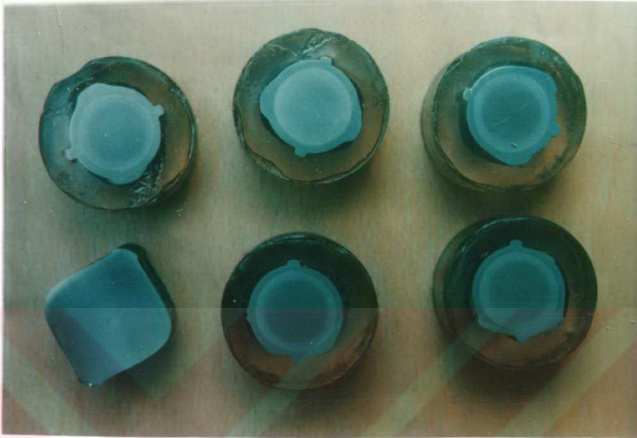
Figure 5.1 Structures of steel bars with 18 mm. bar diameter after different quenching durations.

Depending on some quenching durations, the volume percentages of martensite have been shown in the following Figures 5.2, 5.3, 5.4 for various bar diameters. The amount of martensite increases linearly with the increase of quenching durations.

The transition from thickness of martensite shell to volume percentage of martensite can be calculated as follows:
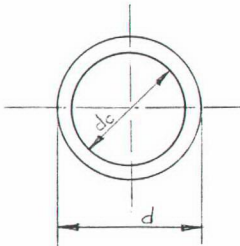
$$A_c = \frac{\pi d_c^2}{4} \qquad (5.1)$$

$$A = \frac{\pi d^2}{4} \qquad (5.2)$$

$$A_S = \frac{\pi d^2}{4} - \frac{\pi d_C{}^2}{4} = \frac{\pi}{4}\left(d^2 - d_C{}^2\right) \tag{5.3}$$

$$\% \text{ Volume of the Martensite Shell} = \frac{A_S}{A}.100 = \frac{\left(d^2 - d_C{}^2\right)}{d^2}.100 \tag{5.4}$$

where,

d_C: diameter of the core (mm.)

d: diameter of the bar (mm.)

A_C: area of the core (mm^2)

A: area of the bar (mm^2)

A_S: area of the martensite shell (mm^2)
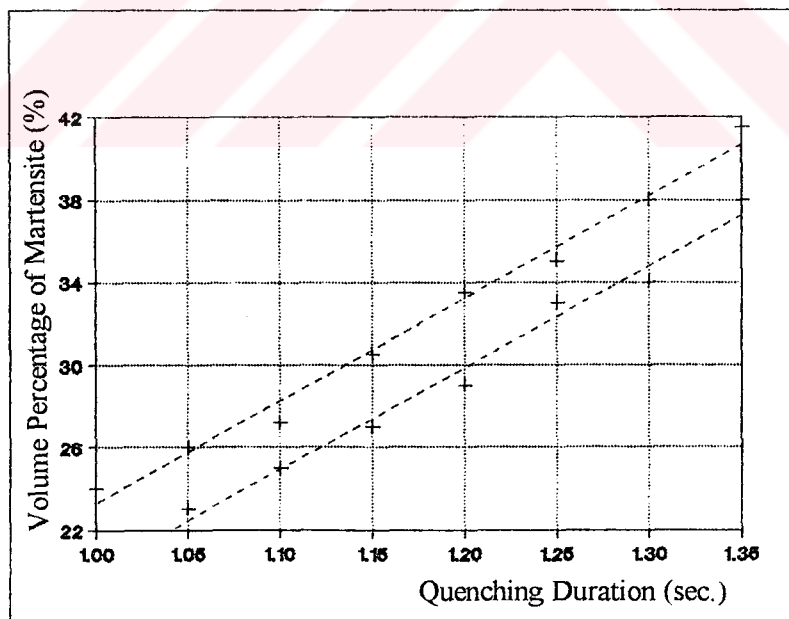
Figure 5.2 Effect of Quenching Time on the Volume Percentage of Martensite of 16 mm. Φ Bar
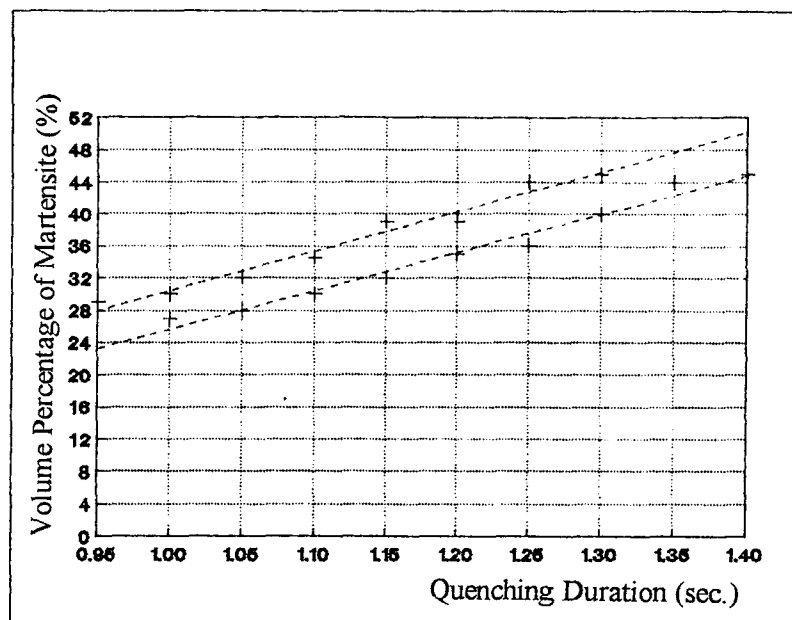
FIGURE 5.3 Effect of Quenching Duration on the Volume Percentage of Martensite
of 18 mm. Φ Bar
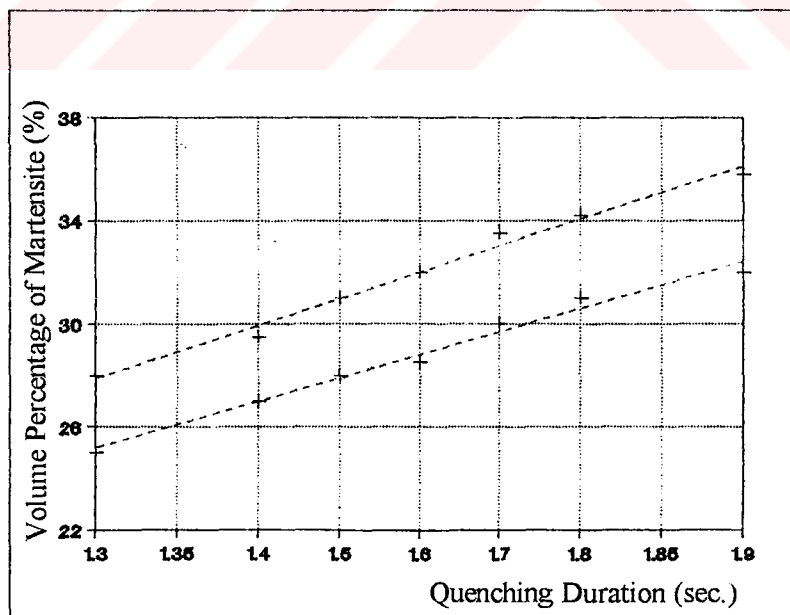
FIGURE 5.4 Effect of Quenching Duration on the Volume Percentage of Martensite
of 22 mm. Φ Bar

5.1.3 Tensile Tests

Specimens have been cut by O_2 + prophene from middle of the bars having 6 m. length as 350 mm. length. Information about tensile test machine was given in the section 5.1.1.

Yield strength, tensile strength and elongation of the bars were obtained from tensile tests. Yield and tensile strength increase linearly by the increase of quenching durations because of the increase of volume percentage of martensite. With increasing of martensite volume yield strength curve approaches to tensile strength curve. This shows that material becomes more brittle. Figures 5.5, 5.6, 5.7, 5.8 show these changes for some bar diameters.

On the other hand, we can also see the change of brittleness occurred by the increase of quenching durations in the Figures 5.9, 5.10, 5.11, 5.12 for different bar diameters: Elongation decreases by the increase of quenching duration.

5.1.4 Determining of the Tempering Temperatures

Real tempering temperature T_r was measured by pyrometer which was put in front of the cooling platform. Pyrometer mark is Impac and type is IP1. Self-tempering temperature decreases with increasing of quenching durations.

Tempering temperature decreases by the increase of martensite shell because heat remained in the volume of core can not increase the temperature of the shell. With decreasing of diameter of the bar, the slope of the quenching duration-tempering temperature curves become more steep (Figures 5.13, 5.14, 5.15, 5.16).

5.1.5 Effect of Tempering Temperature on the Yield, Tensile Strength and Elongation

The increase of tempering temperature decreases yield and tensile strength of the bar linearly. Yield and tensile strength curves separate from each other. In high tempering temperatures, bars have thin martensite shell because martensite layer is tempered by high temperature remained in the core. Figures 5.17, 5.18, 5.19, 5.20, show the changes of yield

and tensile strength for different bar diameters. Yield and tensile strength of the bar decreases with increasing of tempering temperature.

With increasing of martensite layer, heat capacity remained in the bar decreases, then tempering temperature decreases so martensite is tempered by low temperature. Thus toughness and elongation decrease. Figures 5.21, 5.22, 5.23, 5.24 show the changes of elongation for different bar diameters. Elongation of the bar increases with increasing of tempering temperature.
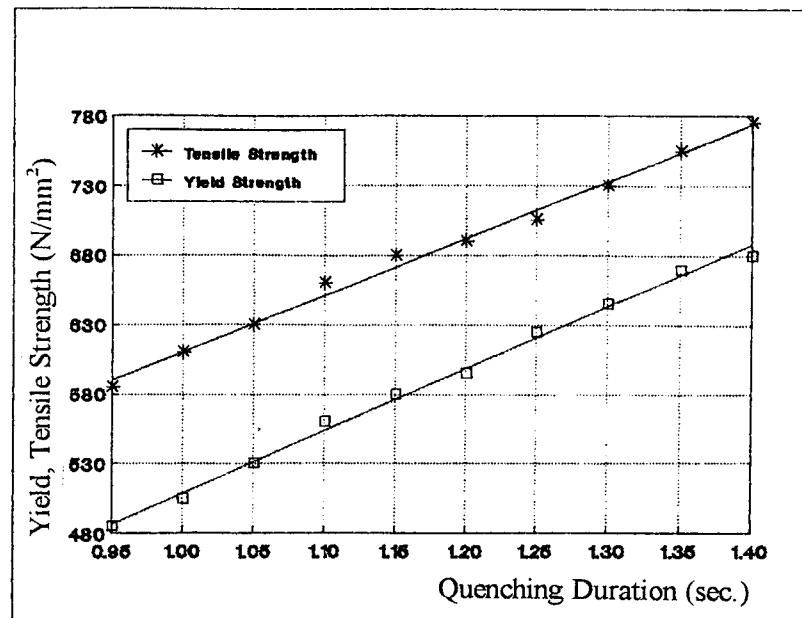
FIGURE 5.5 Effect of Quenching Duration on the Yield and Tensile Strength
of 16 mm. Φ Bar
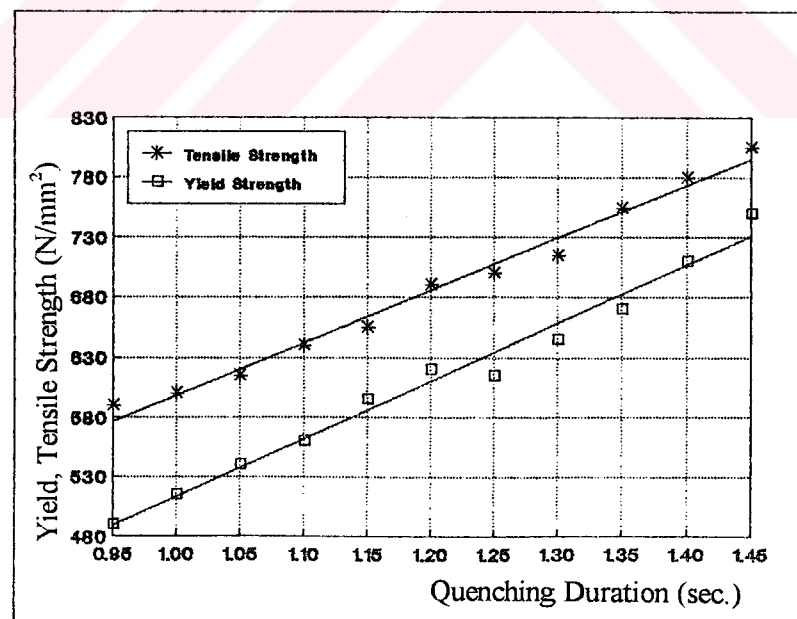
FIGURE 5.6 Effect of Quenching Duration on the Yield and Tensile Strength
of 18 mm. Φ Bar
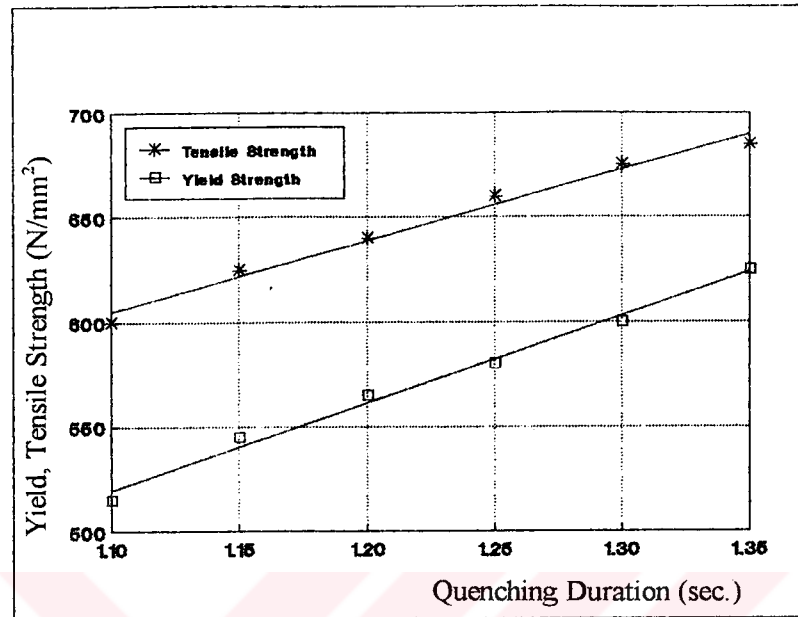
FIGURE 5.7 Effect of Quenching Duration on the Yield and Tensile Strength

of 20 mm. Φ Bar
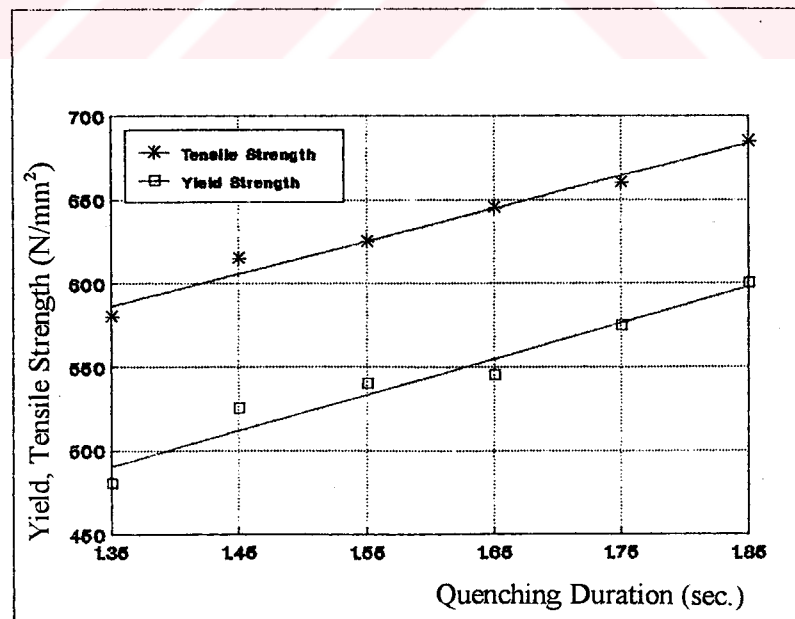
FIGURE 5.8 Effect of Quenching Duration on the Yield and Tensile Strength

of 22 mm. Φ Bar
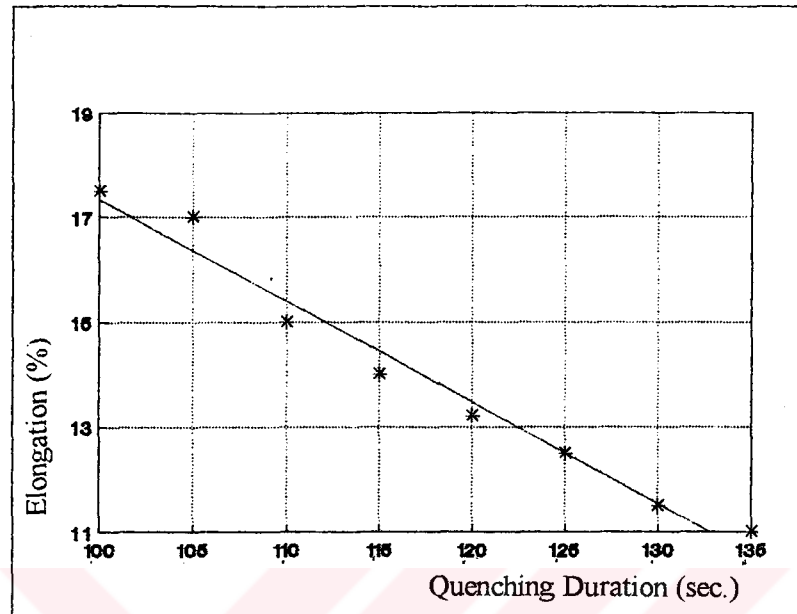
FIGURE 5.9 Effect of Quenching Duration on the Elongation
of 16 mm. Φ Bar
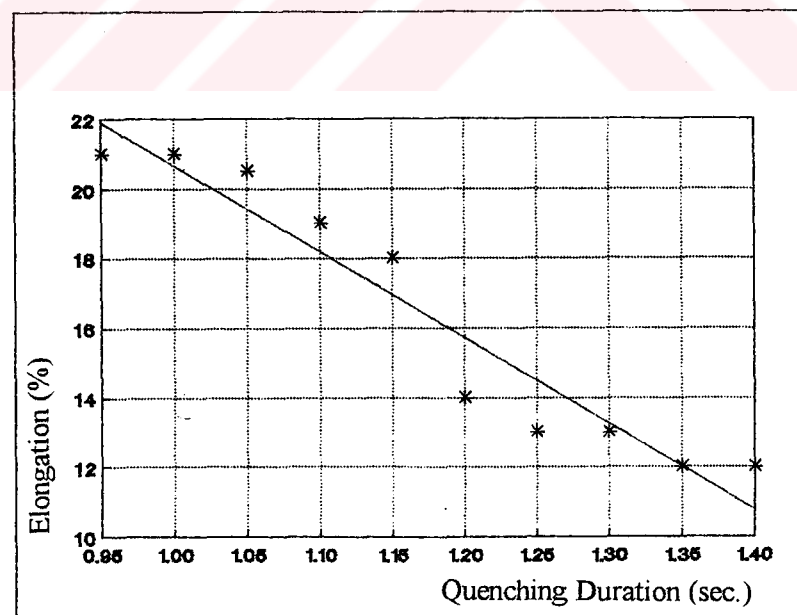
FIGURE 5.10 Effect of Quenching Duration on the Elongation
of 18 mm. Φ Bar
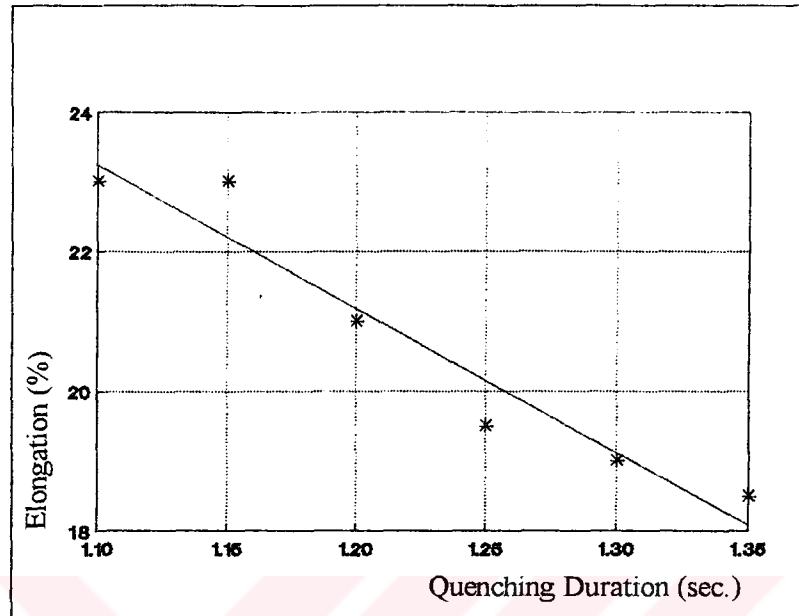
FIGURE 5.11 Effect of Quenching Duration on the Elongation

of 20 mm. Φ Bar
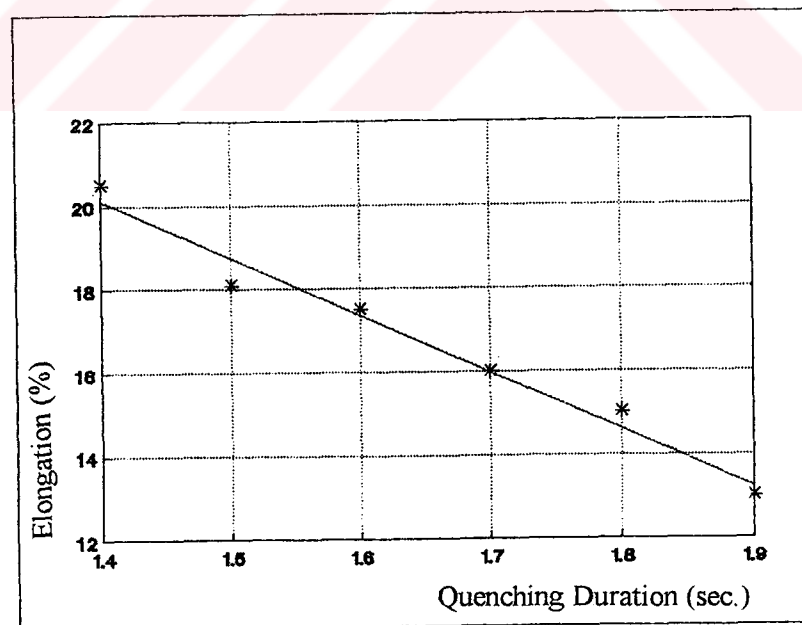
FIGURE 5.12 Effect of Quenching Duration on the Elongation

of 22 mm. Φ Bar
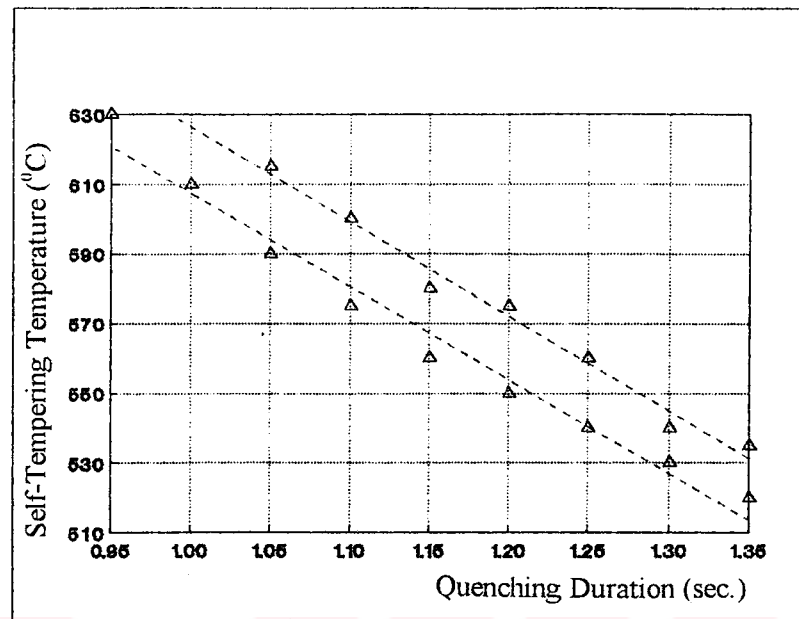
FIGURE 5.13 Effect of Quenching Duration on the Tempering Temperature
of 16 mm. Φ Bar
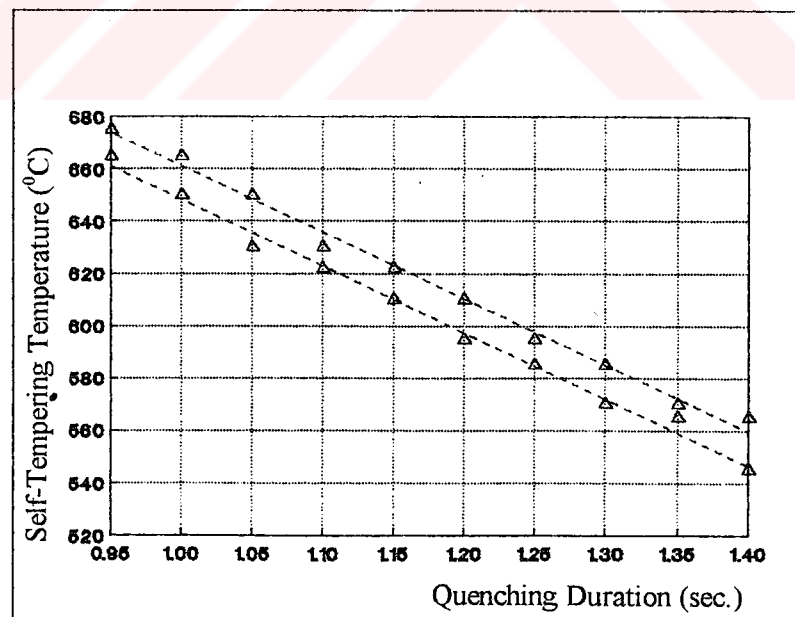
FIGURE 5.14 Effect of Quenching Duration on the Tempering Temperature
of 18 mm. Φ Bar
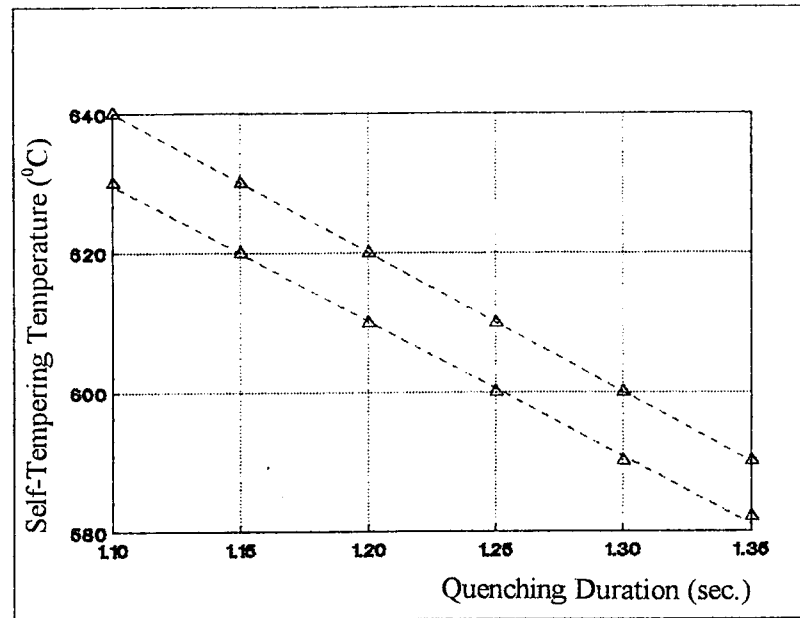
FIGURE 5.15 Effect of Quenching Duration on the Tempering Temperature
of 20 mm. Φ Bar
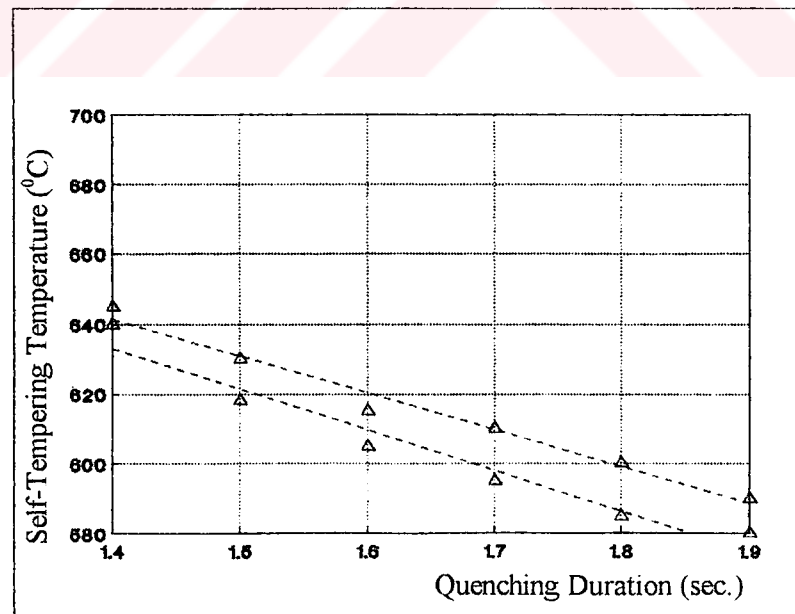
FIGURE 5.16 Effect of Quenching Duration on the Tempering Temperature
of 22 mm. Φ Bar
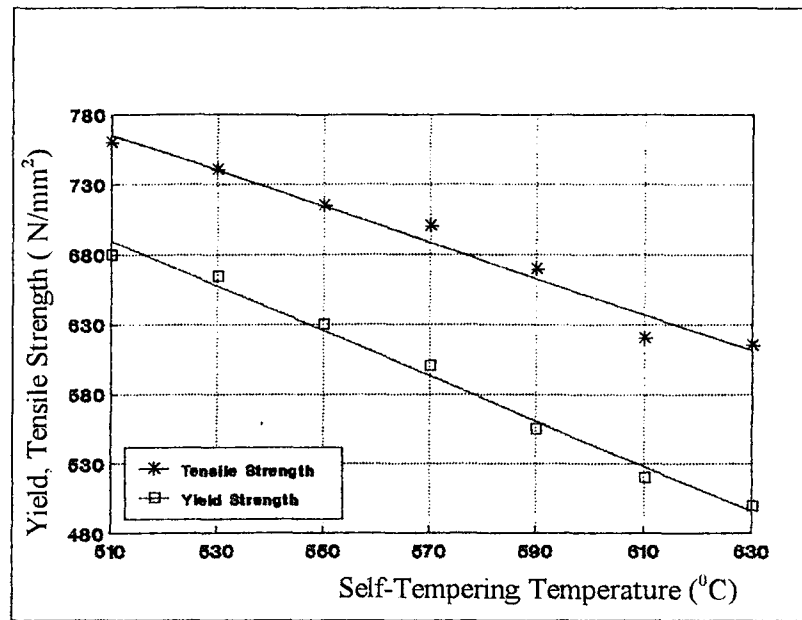
FIGURE 5.17 Effect of Tempering Temperature on the Yield and Tensile Strength
of 16 mm. Φ Bar
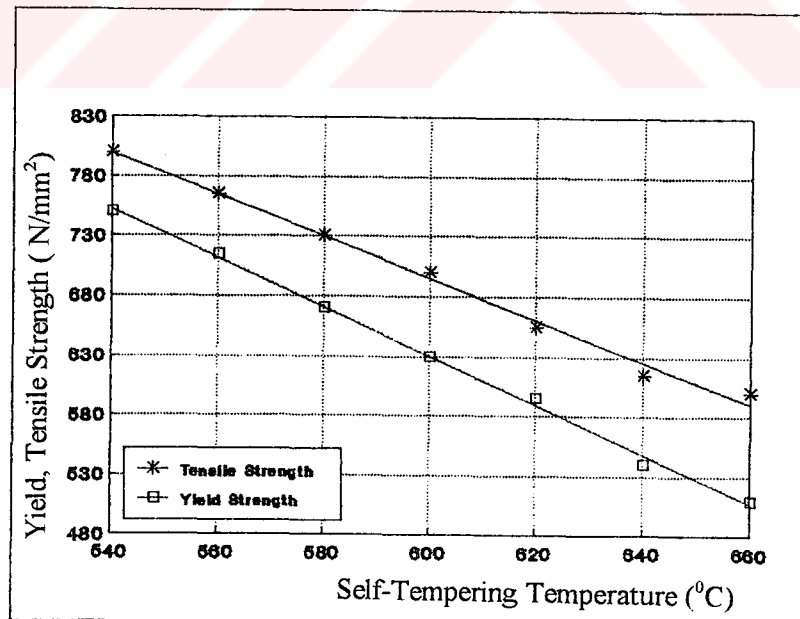
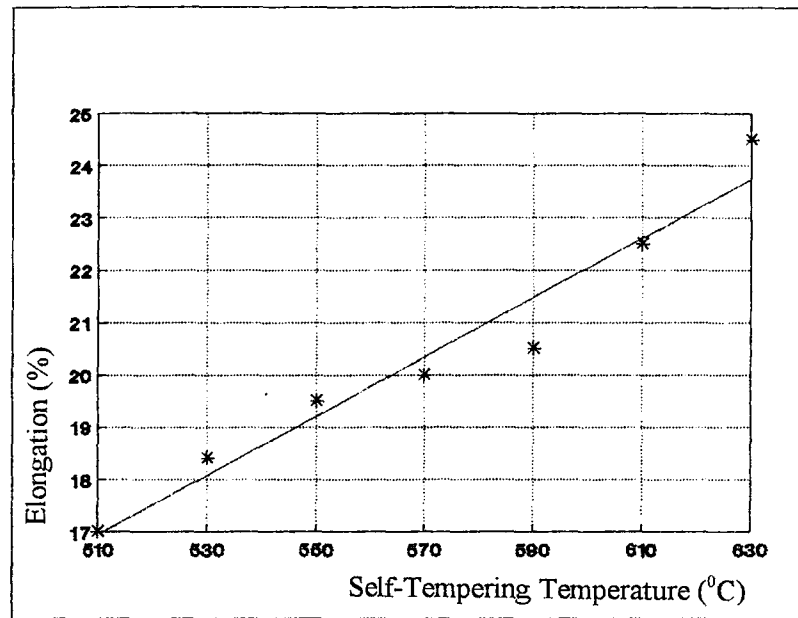FIGURE 5.18 Effect of Tempering Temperature on the Yield and Tensile Strength
of 18 mm. Φ Bar
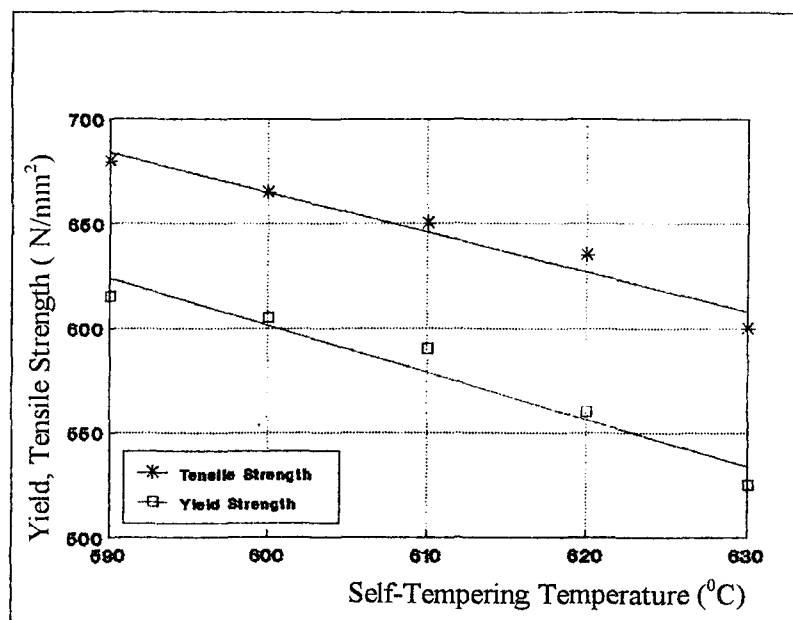
FIGURE 5.19 Effect of Tempering Temperature on the Yield and Tensile Strength
of 20 mm. Φ Bar
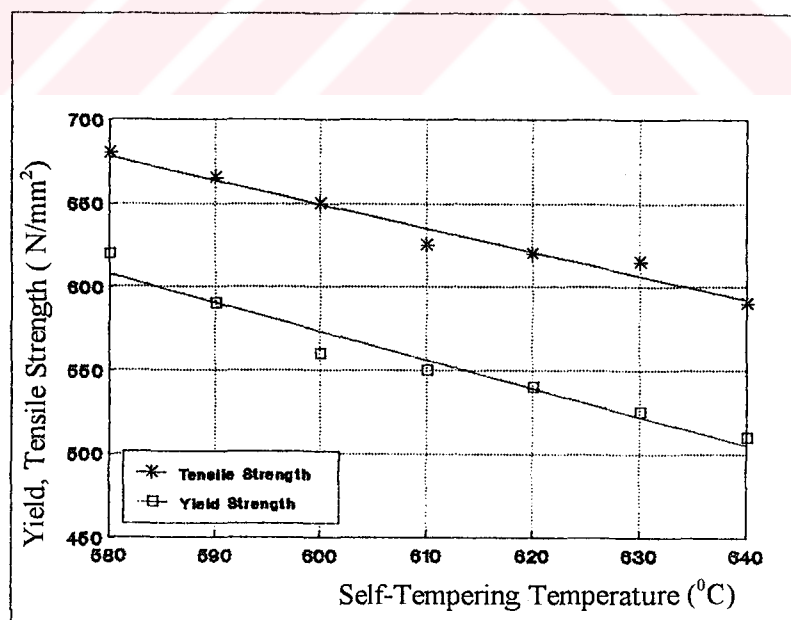
FIGURE 5.20 Effect of Tempering Temperature on the Yield and Tensile Strength
of 22 mm. Φ Bar

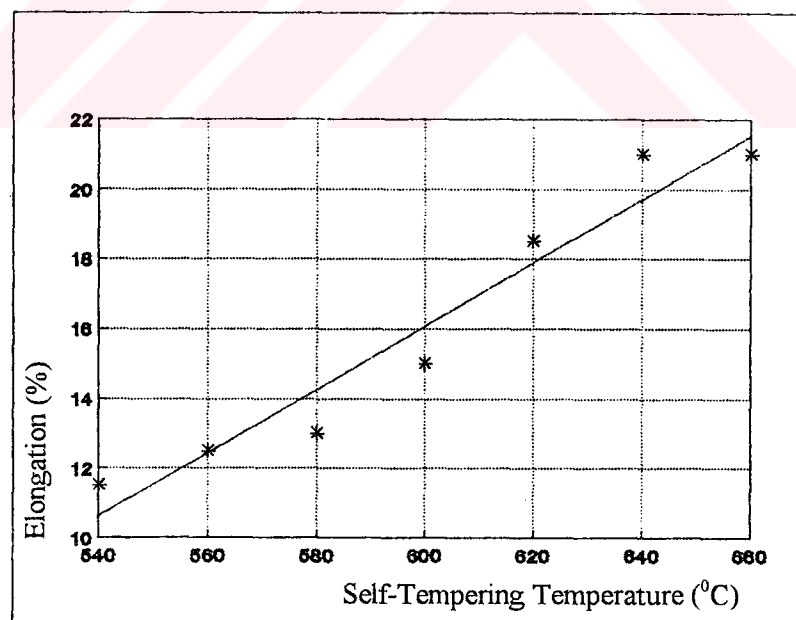FIGURE 5.21 Effect of Tempering Temperature on the Elongation
of 16 mm. Φ Bar

FIGURE 5.22 Effect of Tempering Temperature on the Elongation
of 18 mm. Φ Bar

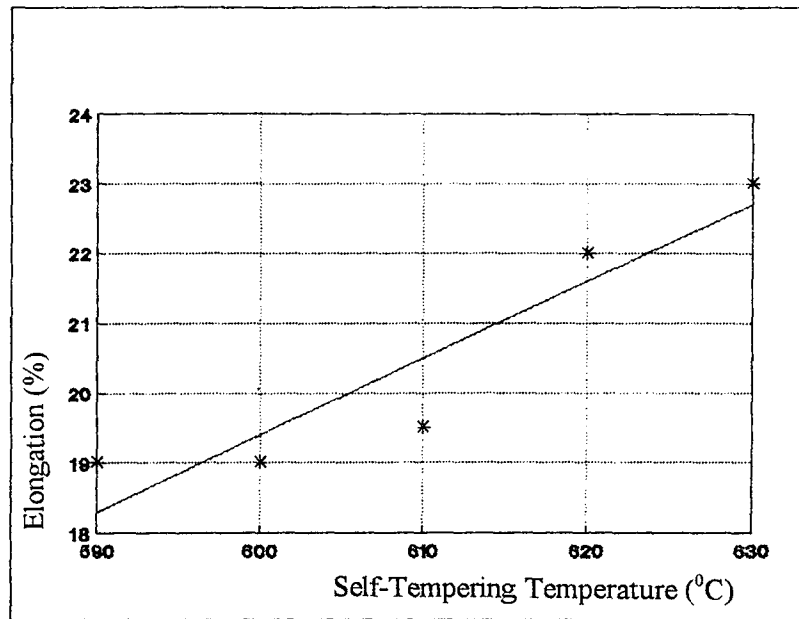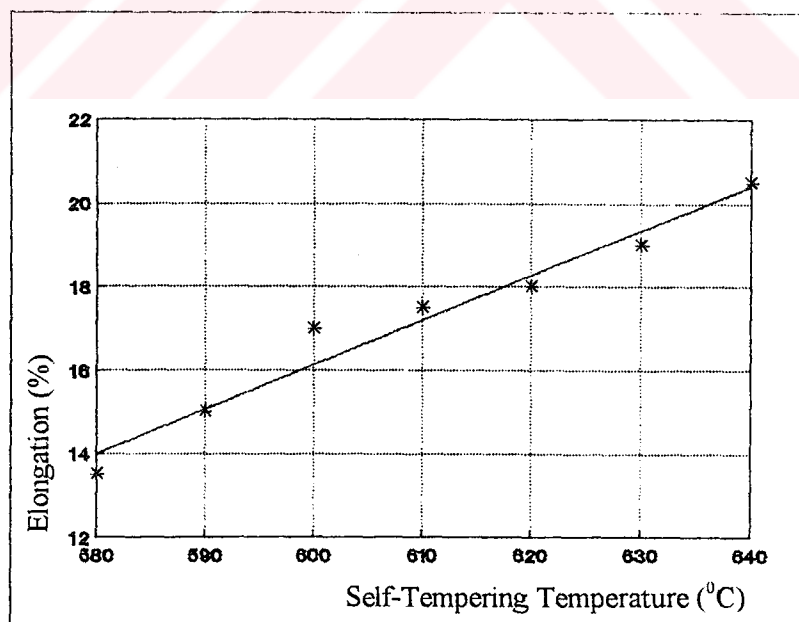FIGURE 5.23 Effect of Tempering Temperature on the Elongation
of 20 mm. Φ Bar

FIGURE 5.24 Effect of Tempering Temperature on the Elongation
of 22 mm. Φ Bar

5.2. Theoretical Study and Results

In finite elements method, steel bars have been modeled as axisymmetric cylindrical shape which has 63 nodes and 40 elements. Heat equations, which were added to equations determining the transition from isothermal time temperature transformation (TTT) to continuous cooling transformation (CCT), were solved by Fortran77 programme. The change of heat capacity, conduction, convection coefficients with temperature and initial temperature, cooling water temperature, air temperature, quenching duration, cooling in the air duration were added as variable. parameters. With this programme the temperature, internal structure, and time were determined for each node. Figures 5.25, 5.26, 5.27, 5.28, 5.29, 5.30 show cooling curves depending on bar diameter and quenching duration.

5.2.1 Internal Structure

With the equations calculating the transition from TTT to CCT, the amount of martensite, ferrite + pearlite and bainite is determined. Figures 5.31, 5.32, 5.33 show the change of the amount of martensite depending on quenching duration and bar diameter. With the increase of quenching duration, volume percentage of martensite increases. On the contrary with increasing of bar diameter volume percentage of martensite decreases, so it affects the toughness of the material. Figures 5.32, 5.33 also show the volume percentages of bainite and ferrite + pearlite in the bar. With the increase of quenching duration, the amount of bainite increases and the amount of ferrite + pearlite decreases. But with the increase of bar diameter the amount of bainite decreases and the amount of ferrite + pearlite increases.

5.2.2 Tempering Temperature

Tempering temperature increases with the increase of bar diameter because heat capacity remained in the core increases the shell temperature. Tempering temperature decreases with the increase of quenching duration. Figures 5.34, 5.35 show the changes of tempering temperature depending on bar diameter and quenching duration.
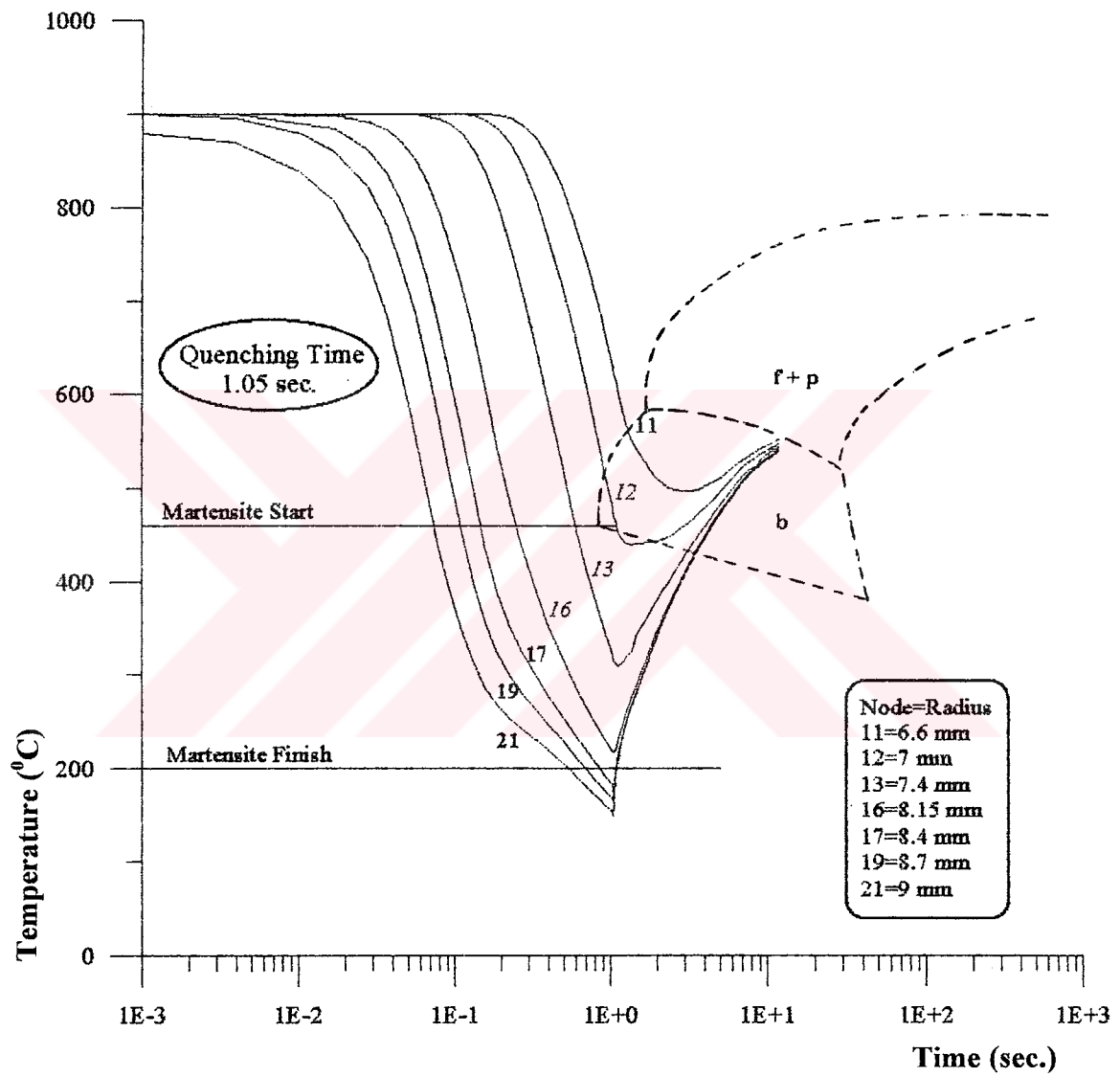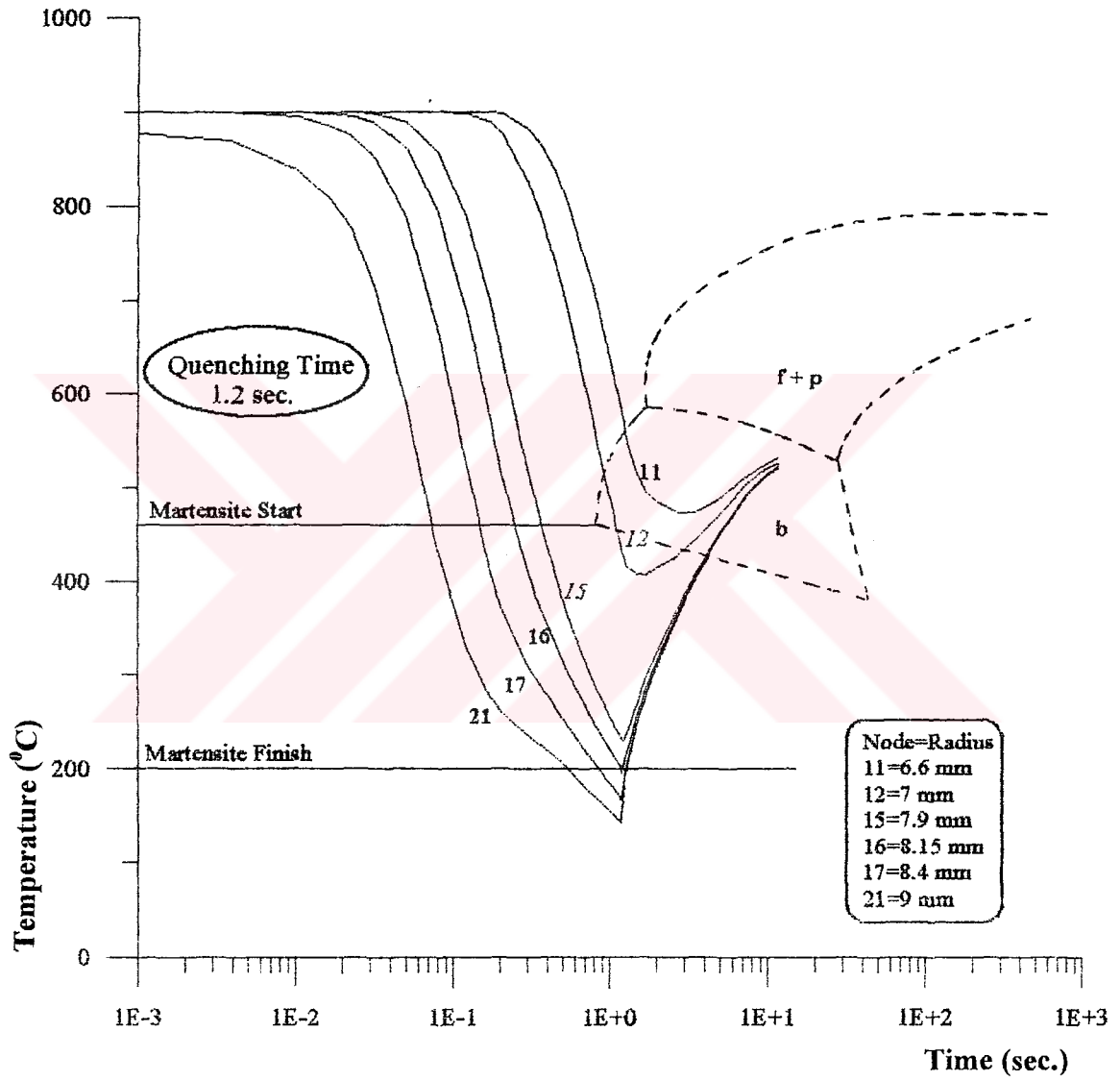
FIGURE 5.25 Cooling Curves in a Quenched 18 mm. Φ Bar
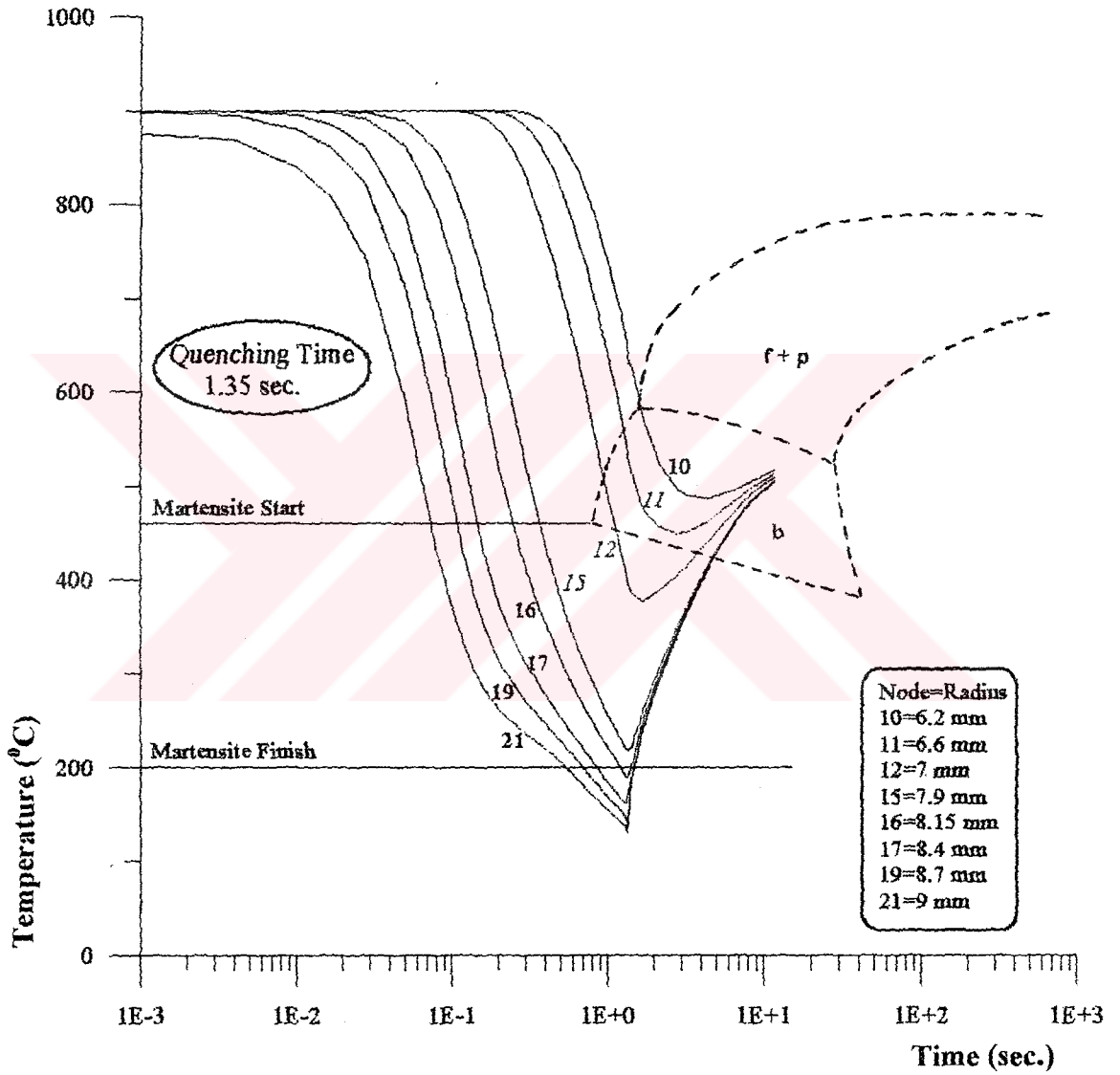
FIGURE 5.26 Cooling Curves in a Quenched 18 mm. Φ Bar
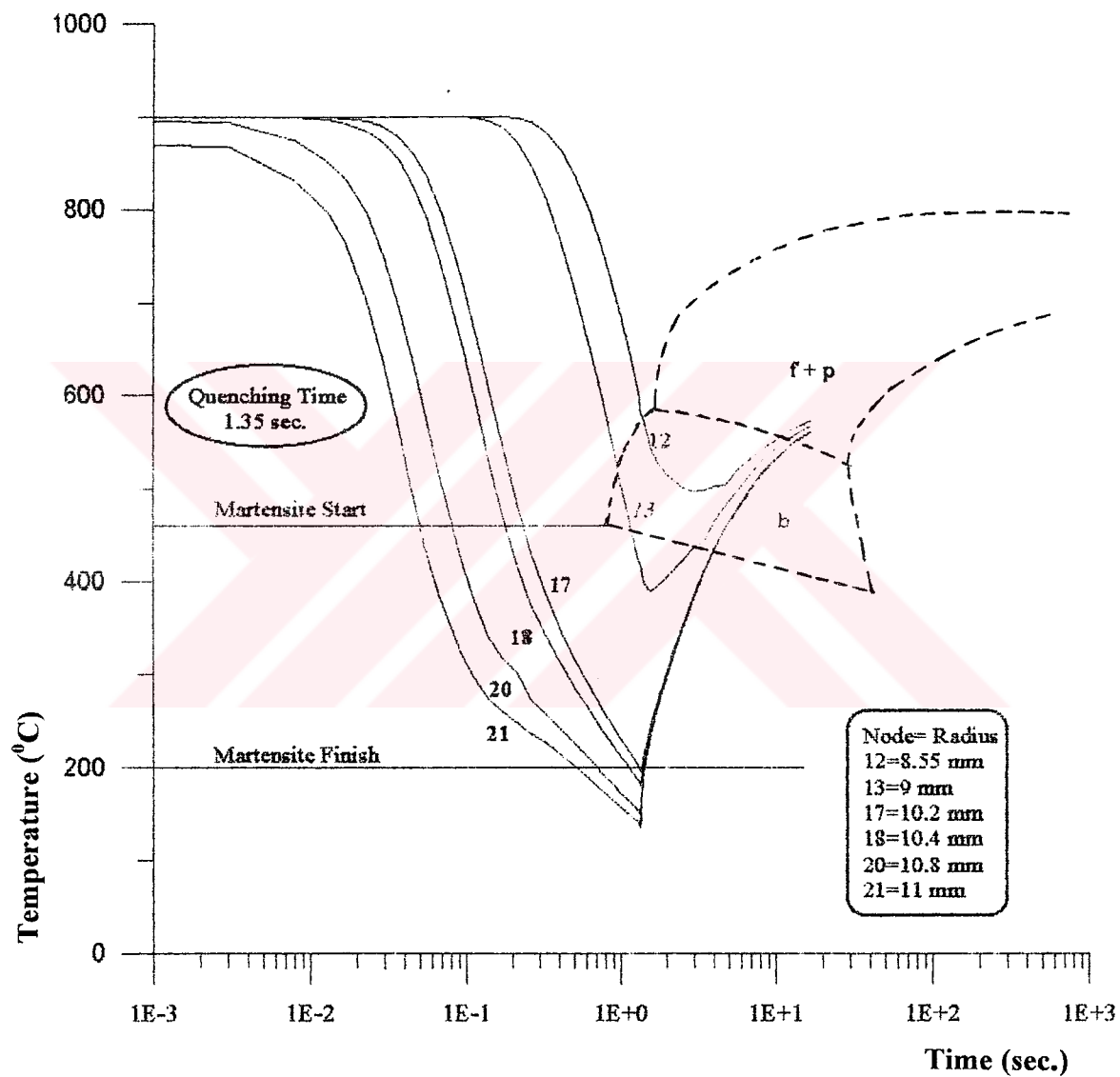
FIGURE 5.27 Cooling Curves in a Quenched 18 mm. Φ Bar
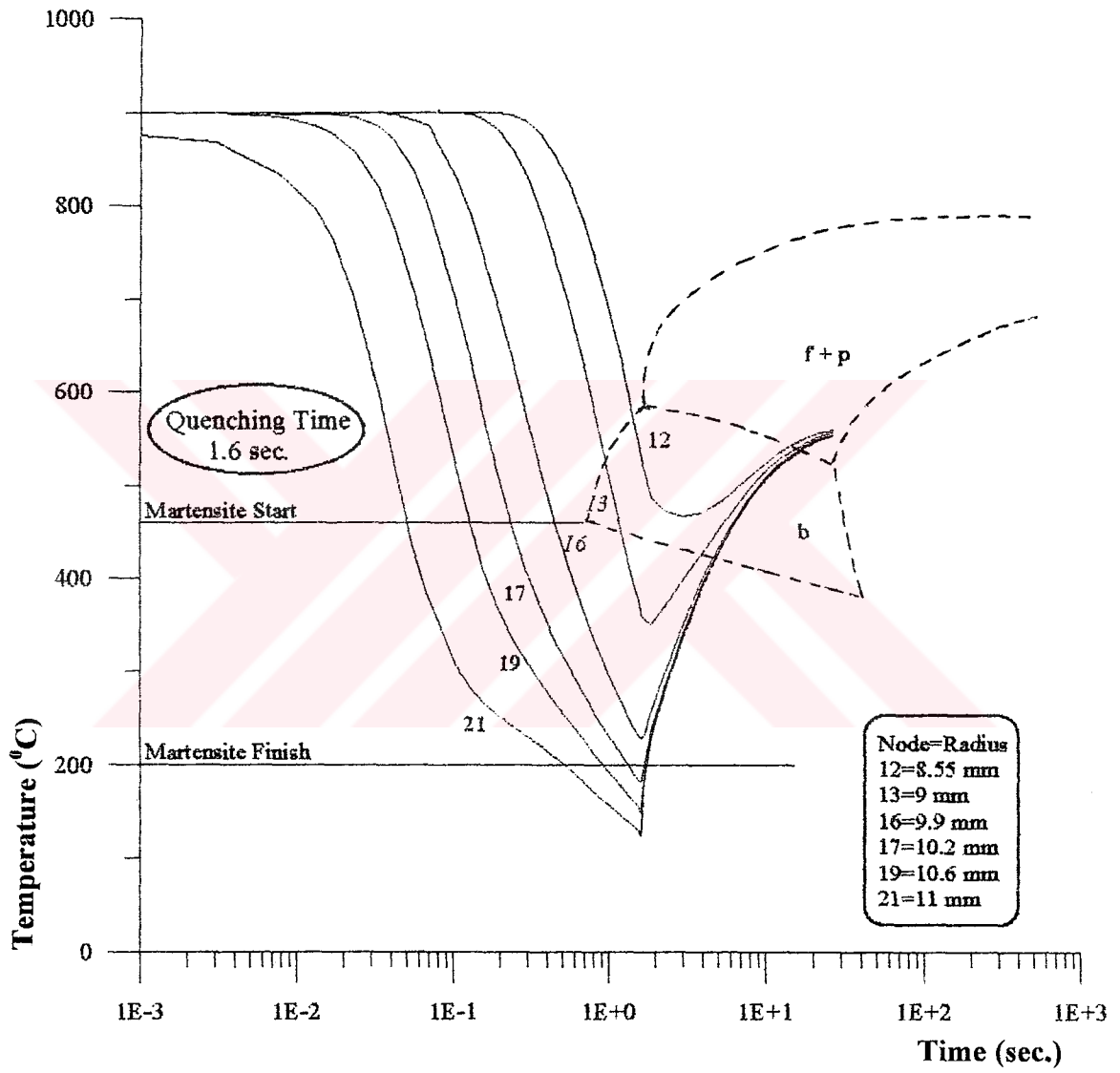
FIGURE 5.28 Cooling Curves in a Quenched 22 mm. Φ Bar
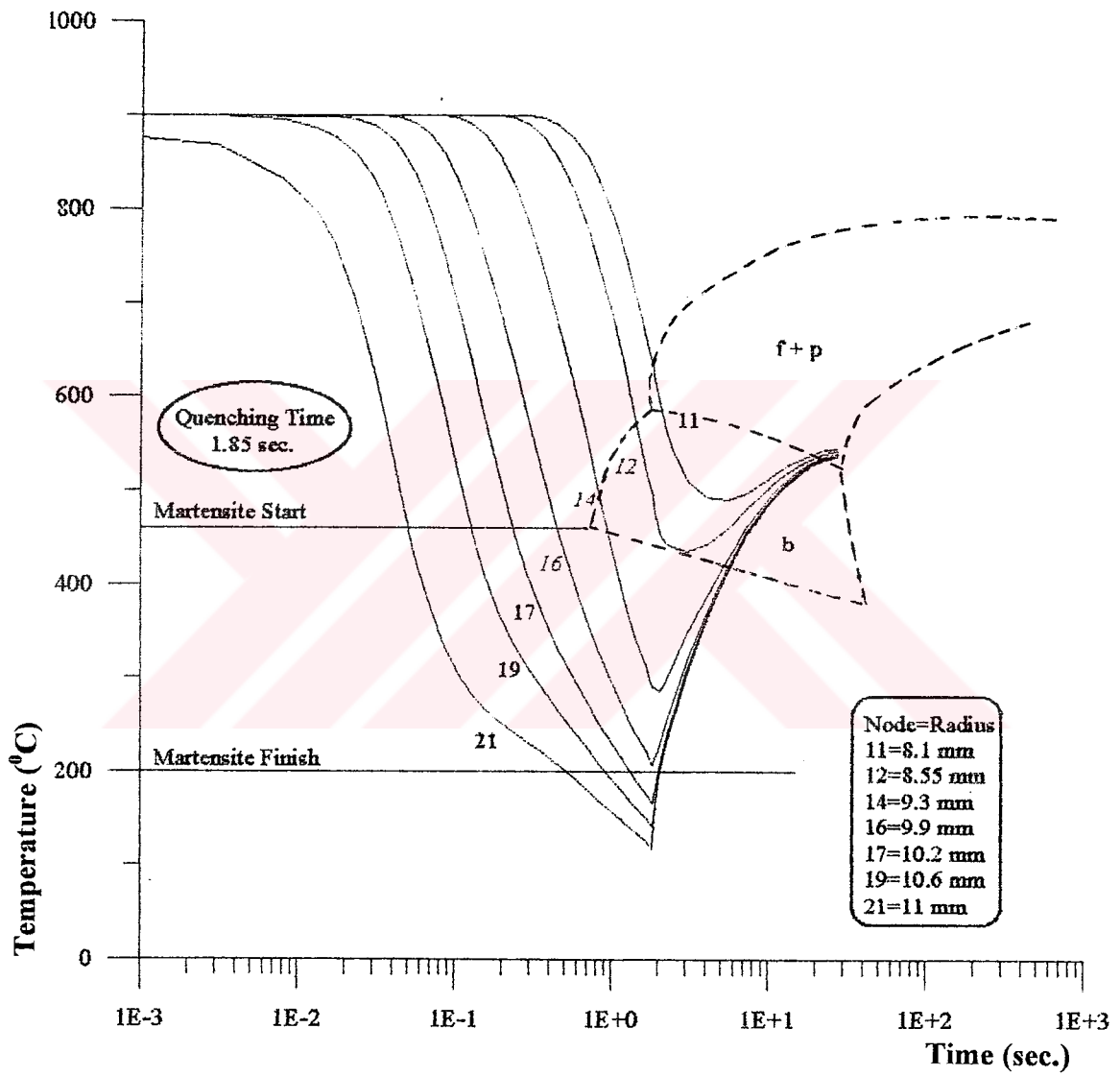
FIGURE 5.29 Cooling Curves in a Quenched 22 mm. Φ Bar
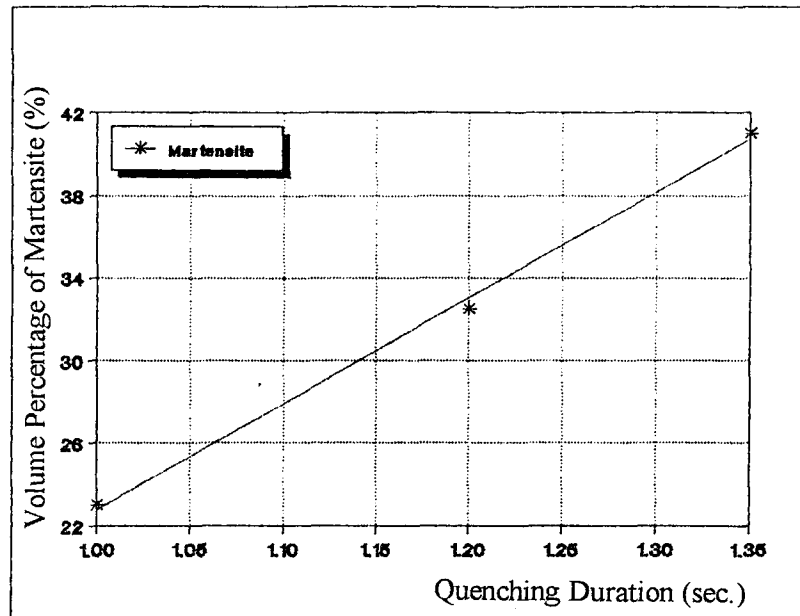
FIGURE 5.30 Cooling Curves in a Quenched 22 mm. Φ Bar

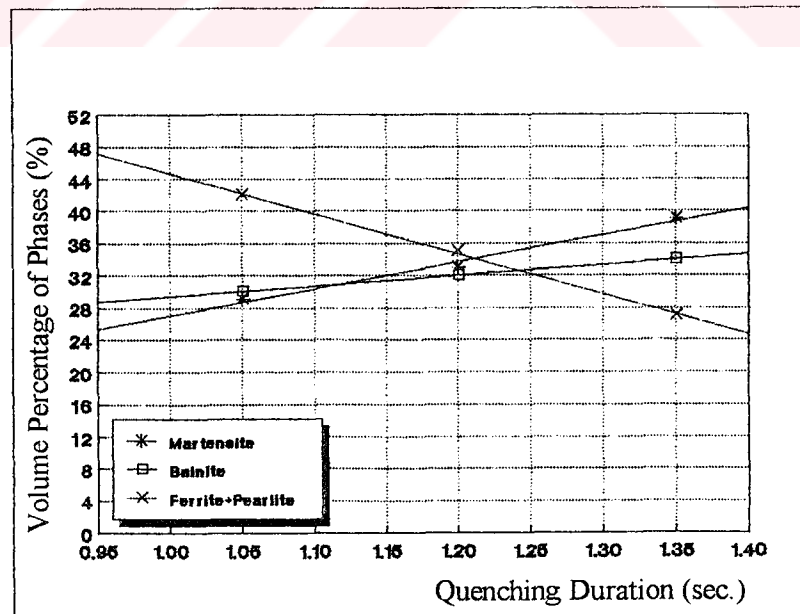FIGURE 5.31 Effect of Quenching Duration on the Internal Structure
of 16 mm. Φ Bar

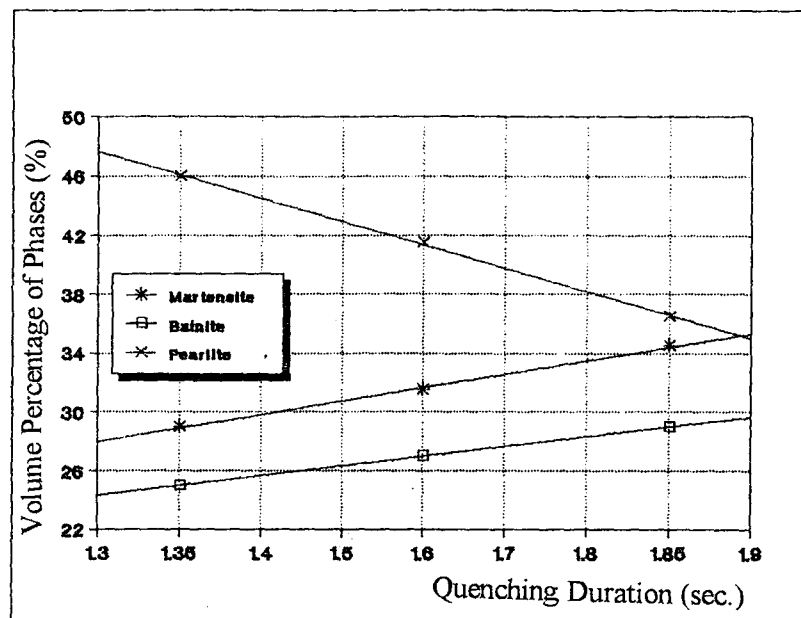FIGURE 5.32 Effect of Quenching Duration on the Internal Structure
of 18 mm. Φ Bar

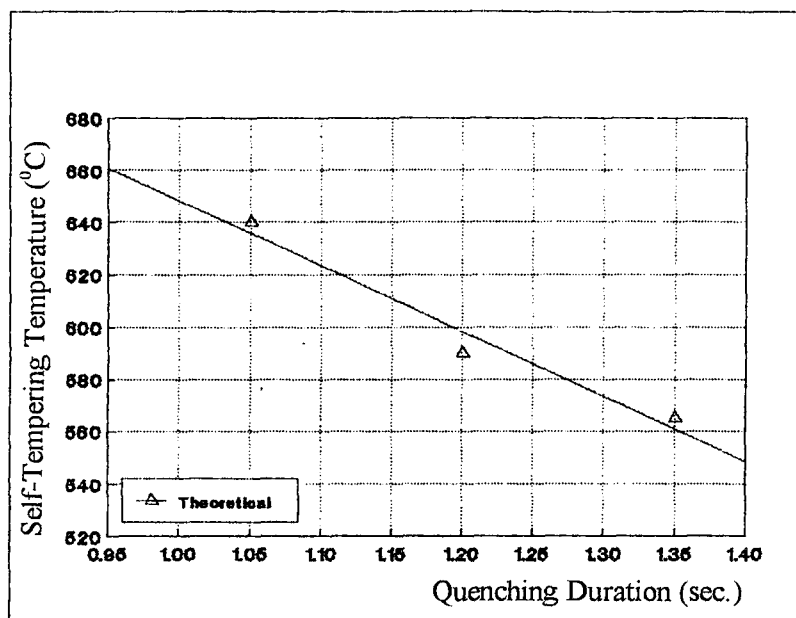FIGURE 5.33 Effect of Quenching Duration on the Internal Structure

of 22 mm. Φ Bar

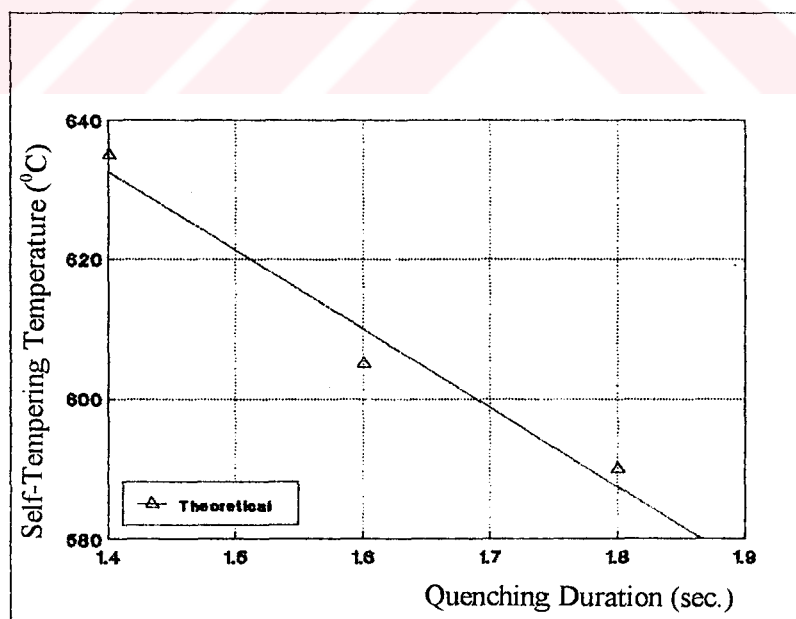FIGURE 5.34 Effect of Quenching Duration on the Tempering Temperature
of 18 mm. Φ Bar

FIGURE 5.35 Effect of Quenching Duration on the Tempering Temperature
of 22 mm. Φ Bar

5.3 Comparison of Theoretical and Experimental Results

Results of the theoretical study support the experimental results. Volume percentages of martensite obtained from theoretical study suit volume percentages of martensite obtained from experimental study. There are some little differences between volume percentage of martensite for the 18 mm. Φ bar diameter obtained from theoretical and experimental study. These differences might have occurred by experimental conditions. For example small changes in cooling water, initial and air temperatures, and cooling bed conditions can affect these results. Results agree with each other in acceptable range. Figures 5.36, 5.37, 5.38 show the comparison of the theoretical and experimental results.

Tempering temperatures obtained from theoretical study are between limits that are obtained from experimental study. With the increase of quenching duration, tempering temperature decreases. On the contrary tempering temperature increases by the increase of bar diameter Figures 5.39, 5.40 show the change of tempering temperatures depending on quenching duration and bar diameter obtained from experimental and theoretical study.

FIGURE 5.36 Comparison of Theoretical and Experimental Volume Percentage
of Martensite of 16 mm. Φ Bar

FIGURE 5.37Comparison of Theoretical and Experimental Volume Percentage
of Martensite of 18 mm. Φ Bar
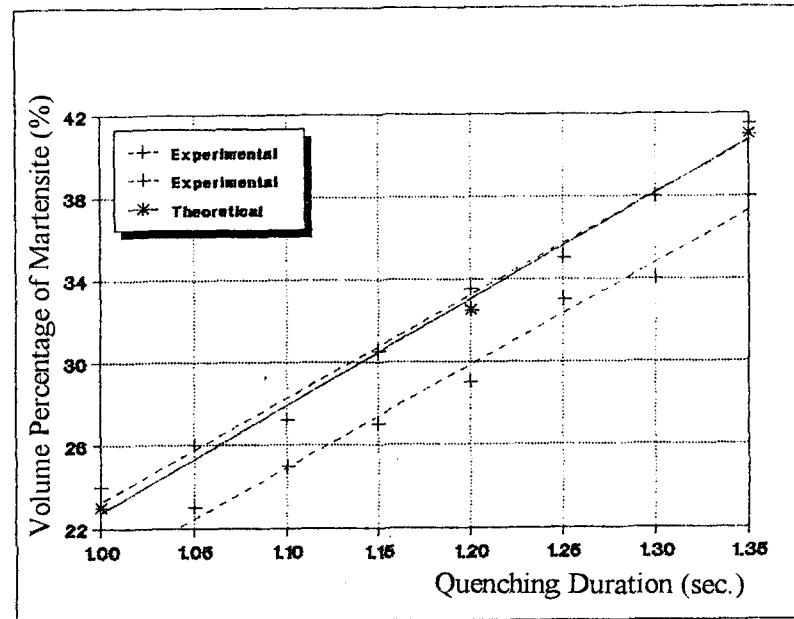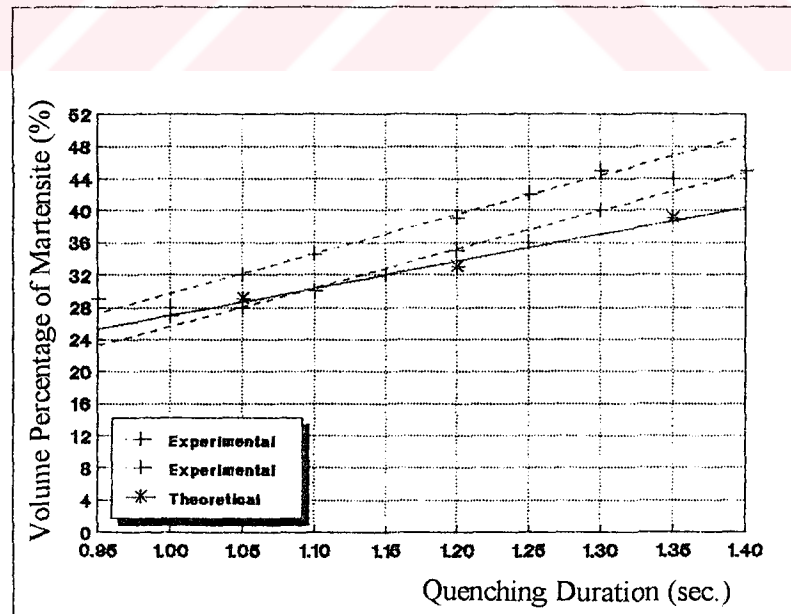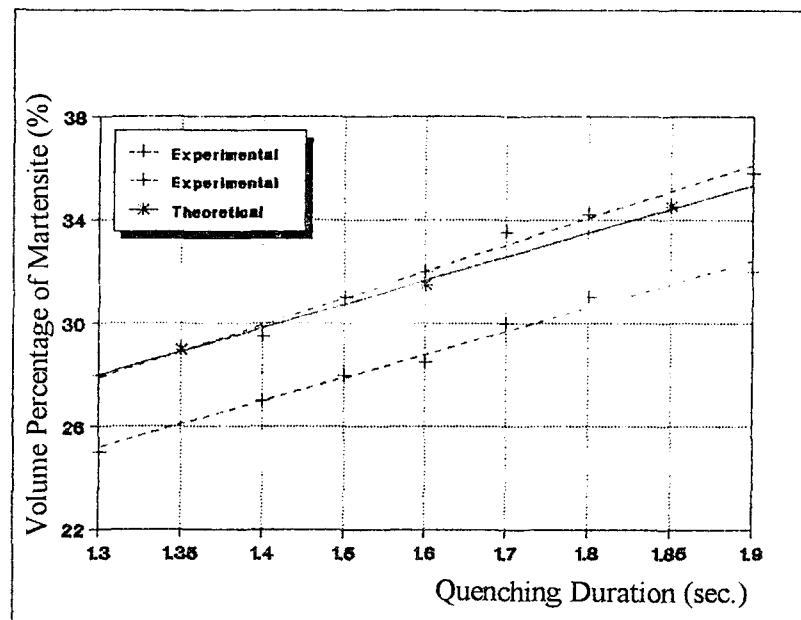
FIGURE 5.38Comparison of Theoretical and Experimental Volume Percentage
of Martensite of 22 mm. Φ Bar

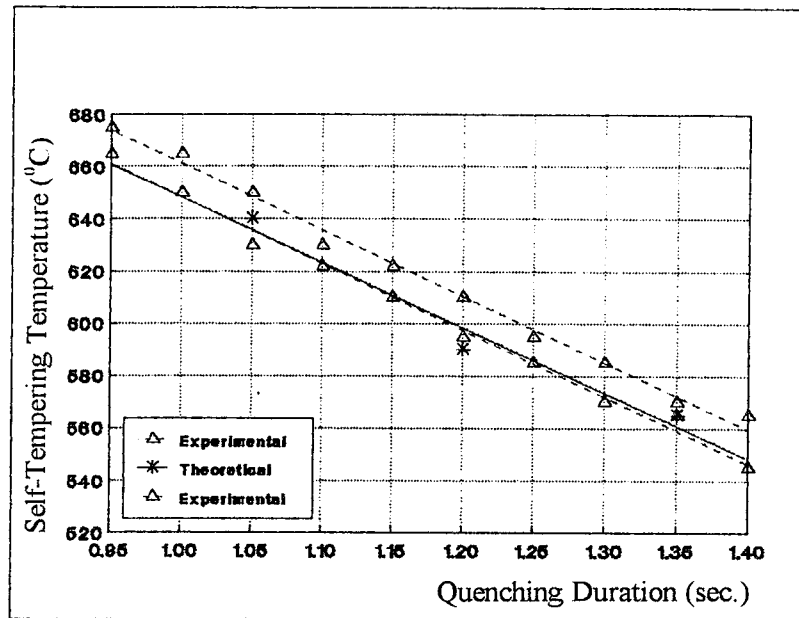FIGURE 5.39 Comparison of Theoretical and Experimental Tempering Temperatures
of Martensite of 18 mm. Φ Bar

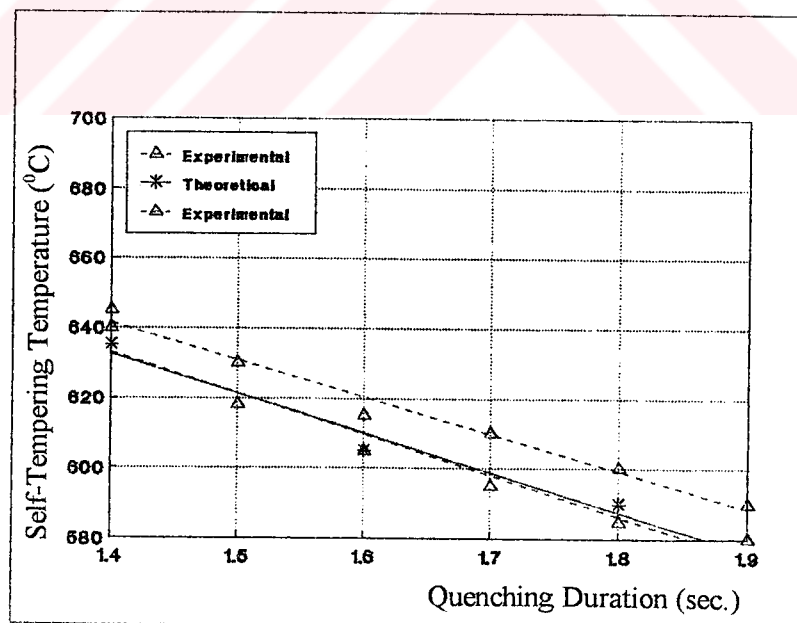FIGURE 5.40 Comparison of Theoretical and Experimental Tempering Temperatures
of Martensite of 22 mm. Φ Bar

CHAPTER SIX
CONCLUSIONS

Results obtained from computer simulation of Tempcore method which used for producing notched steel bars having high yield strength are as follows:

1. Method consists of quenching after hot rolling and then self-tempering procedure. Thus, notched steel bar having high yield strength and suitable for standards can be produced with the compound properties of two structures having different mechanical properties. Internal structure, which occurred in different cooling velocity, was determined in acceptable tolerance by finite elements method.

2. In process, quenching duration is the most important parameter, and with the changebility of this parameter, notched steel bars having high yield strength in appropriate standards can be produced. The change in the internal structure and the effect of this change on the cooling characteristics during quenching was determined by finite elements method sensitively.

3. In experimental studies, it was paid attention to the finish temperatures to be variable. Changes in finish temperature makes it possible the mechanical properties to be varied in a wide range because of its effect on tempering temperatures. This relation can be easily determined by giving finish temperature to the computer programme.

4. Another important parameter of the method is the self-tempering temperature. Self-tempering temperature decreases with the increase in quenching period, so it affects the toughness of the material. Control of this parameter can be achieved by the finishing temperature and quenching time in the programme.

5. As a result, using the finite elements method which supporting the experimental results, some process parameters can be changed more effectively and inexpensively.

REFERENCES

1. Aksoy, T & Önel, K. (1985). Malzeme Bilgisi. İzmir: Dokuz Eylül University Y.N:086

2. Avner, S. H. (1974). Introduction to Physical Metallurgy. Tokyo: Mc Graw-Hill Kogakusha ltd.

3. Bathe, K.J. (1982). Finite Element Procedures in Engineering Analysis. New Jersey: Prentice-Hall Inc.

4. Centre de Recherces Metallurgies (CRM). Tempcore. Liege: Abbaye du Val-Benoit.

5. Dieter, G.E. (1988). Mechanical Metallurgy. London: Mc Graw-Hill Book Company.

6. Economopoulos, M. & Respen, Y. & Lessel, G. & Steffes, G. (1975, No:45). Application of the Tempcore Process to the Fabrication of High Yield Strength Concrete-Reinforcing Bars. CRM Report, pp. 1-17.

7. Economopoulos, M. (1981) The Use of Drastic and Mild Water Cooling Techniques for Controlling Bar and Rod Properties. Metals Society, pp. 76-80.

8. Huebner, K.H. (1982). The Finite Element Method for Engineers. New York: John Wiley-Sons.

9. Killmore, C.R. & Barret, J.F. & Williams, J.G. (1986). Mechanical Properties of High Strength Reinforcing Bar Steels Accelerated Cooled by the Tempcore Process. Metals Society, pp. 541-558.

10. Nath, B. (1974). <u>Fundamentals of Finite Elements for Engineers</u>. London: The Athlone Press of the University of London.

11. Önel, K. (1982). <u>Metallerde Isıl İşleme Giriş</u>. İzmir: Ege University Y.N.: 86.

12. Özsoyeller, L. (1993). Düşük Alaşımlı Nervürlü İnşaat Çeliklerinde Tempcore Yönteminin Mekanik Özelliklere Etkisi. <u>A Thesis Presented to Dokuz Eylül University.</u>

13. The Institute of Metals (1985). <u>Influences on Development of Thermal and Residual Stresses in Quenched Steel Cylinders of Different Dimension</u>. F.R. of Germany: Schröder, R.

14. Simon, P. & Economopoulos, M. & Nilles, P. (1984,March). Tempcore: A New Process for the Production of High Quality Reinforcing Bars. <u>Iron and Steel Engineer</u>, pp. 55-57.

15. Tirupathi, R.C. (1991). <u>Introduction to Finite Elements in Engineering</u>. New Jersey: Prentice Hall Englewood Cliffs.

16. Toparlı, M. (1990). Calculation of Residual Stresses in Cylindirical Steel Bars by Finite Elements Method. <u>A Thesis Presented to Dokuz Eylül University</u>.

17. Vlack, L.H.Y. (1964). <u>Element of Materials Science</u>. Tokyo: Addison-Wesley Publishing Company, Inc.

18. Yu, H.J. (1977). Berechung von Abkühlungs-, Umwandlungs-, Schweiss-, Sowie Verformungseigenspannungen mit Hilfe der Methode der Finiten Elemente. <u>Tag derMündlichen Prüfung</u>. Universitat Karlsruhe.

19. Zienkiewicz, O.C. (1982). <u>The Finite Element Method</u>. London: Mc Graw Hill Book Company.